Published OnlineFirst September 18, 2017; DOI: 10.1158/2159-8290.CD-17-0682

RESEARCH ARTICLE

Exploiting Drug Addiction Mechanisms to Select against MAPKi-Resistant Melanoma

Aayoung Hong[1,2,3], Gatien Moriceau[1,3], Lu Sun[1,3], Shirley Lomeli[1,3], Marco Piva[1,3], Robert Damoiseaux[2,3,4], Sheri L. Holmen[5], Norman E. Sharpless[6], Willy Hugo[1,3], and Roger S. Lo[1,2,3,4]

ABSTRACT

Melanoma resistant to MAPK inhibitors (MAPKi) displays loss of fitness upon experimental MAPKi withdrawal and, clinically, may be resensitized to MAPKi therapy after a drug holiday. Here, we uncovered and therapeutically exploited the mechanisms of MAPKi addiction in MAPKi-resistant *BRAF*^{MUT} or *NRAS*^{MUT} melanoma. MAPKi-addiction phenotypes evident upon drug withdrawal spanned transient cell-cycle slowdown to cell-death responses, the latter of which required a robust phosphorylated ERK (pERK) rebound. Generally, drug withdrawal–induced pERK rebound upregulated p38–FRA1–JUNB–CDKN1A and downregulated proliferation, but only a robust pERK rebound resulted in DNA damage and parthanatos-related cell death. Importantly, pharmacologically impairing DNA damage repair during MAPKi withdrawal augmented MAPKi addiction across the board by converting a cell-cycle deceleration to a caspase-dependent cell-death response or by furthering parthanatos-related cell death. Specifically in MEKi-resistant *NRAS*^{MUT} or atypical *BRAF*^{MUT} melanoma, treatment with a type I RAF inhibitor intensified pERK rebound elicited by MEKi withdrawal, thereby promoting a cell death–predominant MAPKi-addiction phenotype. Thus, MAPKi discontinuation upon disease progression should be coupled with specific strategies that augment MAPKi addiction.

SIGNIFICANCE: Discontinuing targeted therapy may select against drug-resistant tumor clones, but drug-addiction mechanisms are ill-defined. Using melanoma resistant to but withdrawn from MAPKi, we defined a synthetic lethality between supraphysiologic levels of pERK and DNA damage. Actively promoting this synthetic lethality could rationalize sequential/rotational regimens that address evolving vulnerabilities. *Cancer Discov; 8(1); 74–93. ©2017 AACR.*

See related commentary by Stern, p. 20.

[1]Division of Dermatology, Department of Medicine, University of California, Los Angeles, California. [2]Department of Molecular and Medical Pharmacology, University of California, Los Angeles, California. [3]David Geffen School of Medicine, University of California, Los Angeles, California. [4]Jonsson Comprehensive Cancer Center, University of California, Los Angeles, California. [5]Huntsman Cancer Institute and Department of Surgery, University of Utah Health Sciences Center, Salt Lake City, Utah. [6]Lineberger Comprehensive Cancer Center, University of North Carolina School of Medicine, Chapel Hill, North Carolina.

Note: Supplementary data for this article are available at Cancer Discovery Online (http://cancerdiscovery.aacrjournals.org/).

A. Hong and G. Moriceau contributed equally to this article.

Corresponding Author: Roger S. Lo, University of California, Los Angeles, 52-121 CHS, 10833 Le Conte Avenue, Los Angeles, CA 90095-1750. E-mail: rlo@mednet.ucla.edu

doi:10.1158/2159-8290.CD-17-0682

Published OnlineFirst September 18, 2017; DOI: 10.1158/2159-8290.CD-17-0682

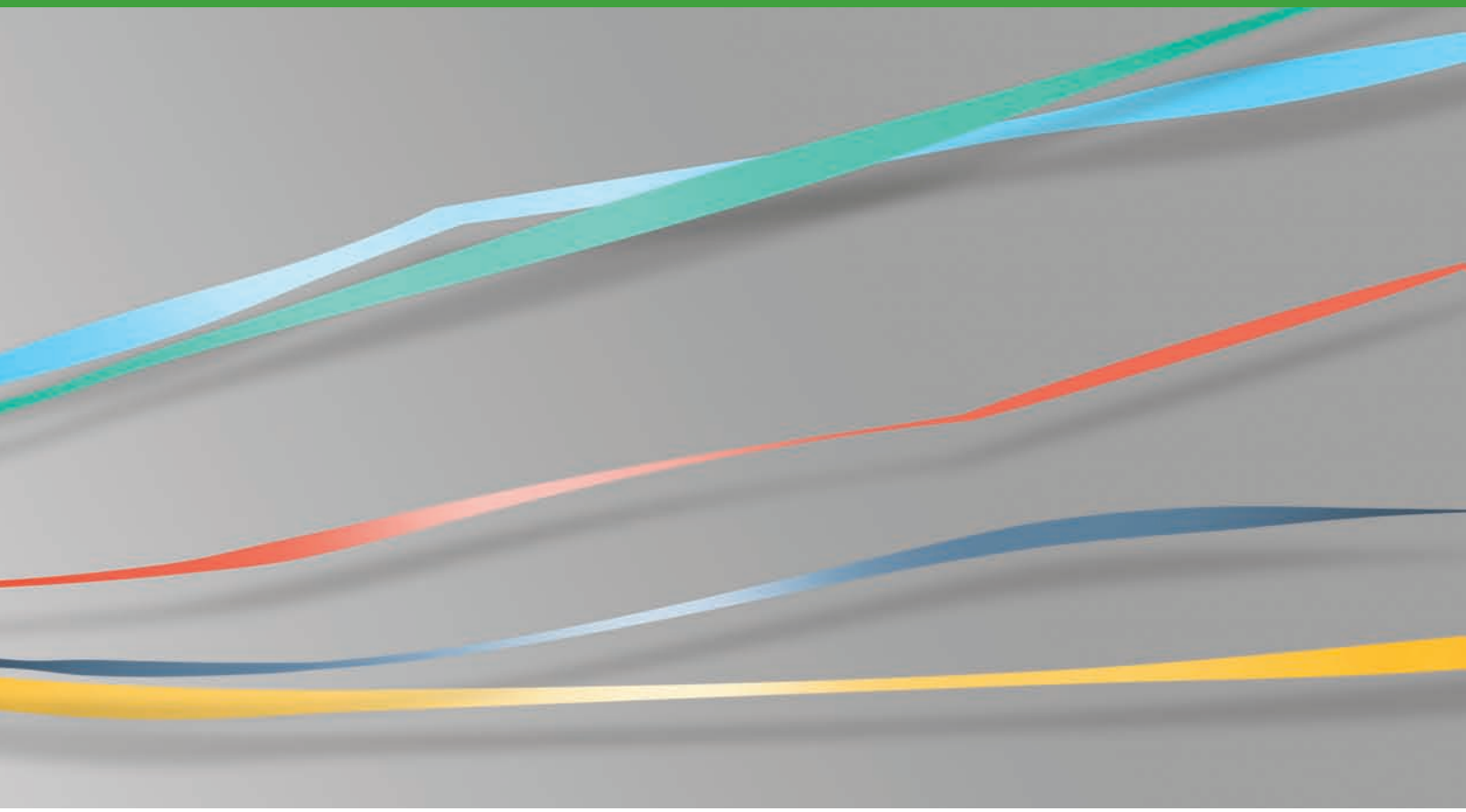

INTRODUCTION

The combination of BRAF inhibitors plus MEK inhibitors (BRAFi + MEKi) extends the survival benefits of BRAFi monotherapy in *BRAF*^{V600}-mutant melanoma by counteracting MAPK-reactivating resistance mechanisms (1–9). However, acquired resistance to BRAFi + MEKi is the norm rather than the exception. In cell line and patient-derived xenograft (PDX) models of *BRAF*^{V600}-mutant melanoma adapted to BRAFi monotherapy, loss-of-fitness due to BRAFi withdrawal in a process termed drug addiction has been documented (2, 10). Moreover, the magnitude of drug addiction increases with adaptation to BRAFi + MEKi (2). Regardless of the extent of drug addiction, rebound phosphorylated ERK (pERK) levels induced by MAPKi (BRAFi or BRAFi + MEKi) withdrawal seemed critical for this phenotype, because a low dose of ERK inhibitor (ERKi) was sufficient to block this pERK rebound and reversed drug addiction (2). However, how pERK rebound mediates tumor cell cycle deceleration and/or cell death is unknown. Identifying the factor(s) that, together with pERK rebound, incite tumor cell death or regression (rather than mere tumor stabilization or transient tumor cytostasis) may inform potential clinical strategies.

Anecdotal case series of patients with advanced *BRAF*^{V600}-mutant melanoma suggest that rechallenge with a MAPKi, after evidence of disease progression and a brief drug holiday, can lead to clinical benefits, including objective tumor regression and enhanced life quality (11–16). More recently, a prospective clinical trial demonstrated that, following an interval of at least 12 weeks since disease progression and off MAPKi, rechallenge with BRAFi + MEKi led to 32% partial responses and 40% disease stabilization (17). Thus, an intentional drug holiday may select against MAPKi-resistant melanoma, leading to a resensitization phenomenon. Maximizing this counter-selection may lead to greater rates of resensitization and, if applied against microscopic resistance earlier during MAPKi therapy, could lead to longer durations of response or disease control.

Currently, MAPKi therapy is clinically approved only for patients with advanced *BRAF*^{V600}-mutant melanoma. This is because type I RAF inhibitors (vemurafenib and dabrafenib) specifically inhibit monomeric BRAF^{V600} mutants (18) but paradoxically activate the MAPK pathway in NRAS-mutant and/or dimeric RAF-active melanoma (19–22). MEKi monotherapy has clear clinical activity against advanced *BRAF*^{V600}-mutant melanoma (23) but more limited activity against advanced *NRAS*^{MUT} melanoma (24). Thus, strategies against MEKi-resistant melanoma, including *NRAS*^{MUT} melanoma specifically and other subsets of melanoma with potential MAPKi sensitivity, may have clinical utility.

In this study, we sought to understand the basis of variable cellular responses (cell cycle versus death) to drug withdrawal in MAPKi-resistant melanoma. We also provided *in vivo* (PDX and murine melanoma in immune competent mice) proof-of-concept evidence that specific therapeutic approaches could potentially augment MAPKi addiction by favoring tumor cell death over transient cell-cycle suppression. Using three independent MEKi-resistant melanoma models with *NRAS*^{MUT}

Published OnlineFirst September 18, 2017; DOI: 10.1158/2159-8290.CD-17-0682

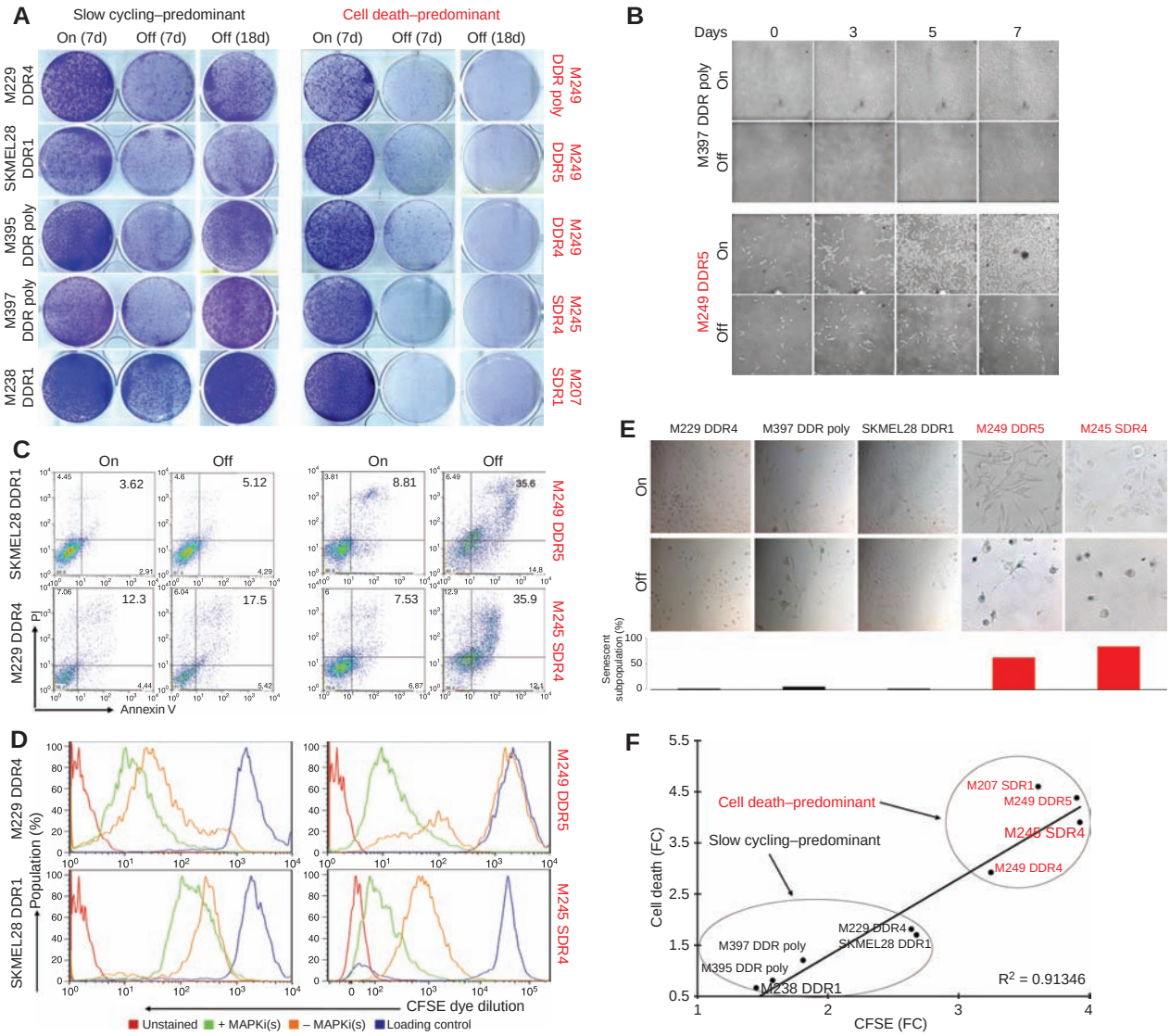

Figure 1. MAPKi-resistant melanomas display distinct drug-addiction phenotypes characterized by slow-cycling versus cell-death responses. **A,** Clonogenic growth of double-drug resistant or DDR (*BRAF*^{MUT}) or single-drug resistant or SDR (*NRAS*^{MUT}) melanoma cell lines plated 24 hours with BRAFi (vemurafenib) + MEKi (selumetinib) at 1 μmol/L or MEKi (trametinib) at 0.1 μmol/L followed by 7 days with (on) or 7 and 18 days without (off) inhibitor. **B,** Temporal vital images of MAPKi-resistant or R-lines on or off BRAFi + MEKi. **C–E,** Percentages of Annexin-V/PI-positive dead cells (**C**), CFSE dye dilution patterns (**D**), and levels of SA-βgal staining (**E**) in R-lines on or off MAPKi(s) for 6 days. Loading control (**D**) refers to the intensity of the CFSE dye initially loaded into the cells. **F,** Correlation between fold changes (FC) in CFSE dye dilution and % cell death off vs. on MAPKi(s). PI, propidium iodide.

or atypical *BRAF* mutations, we derived data suggesting that MAPKi addiction is not exclusive to *BRAF*^{V600}-mutant melanoma and may be a hallmark of MAPKi-resistant melanoma.

RESULTS

Depth of Drug Addiction in Resistant Melanoma Is Determined by Slow-Cycling versus Cell-Death Responses to MAPKi Withdrawal

Previously, we have shown that acquired MAPKi resistance mechanisms vary in their degrees of ERK reactivation (1, 3, 25) and that the levels of MAPKi addiction correlate with the degrees of pERK rebound upon drug(s) withdrawal (2). To assess the spectrum of variations in the MAPKi-addiction phenotype, we analyzed the cellular responses of *BRAF*^{V600}-mutant, double-drug resistant (DDR) melanoma cell lines to BRAFi + MEKi withdrawal. We extended our analysis to *NRAS*^{Q61}-mutant melanoma sublines with acquired MEKi resistance [M207 and M245 single-drug resistant (SDR)]. All 10 melanoma cell lines with diverse mechanisms (Supplementary Fig. S1A) of acquired MAPKi resistance (R-lines) displayed MAPKi addiction (Fig. 1A). This loss-of-fitness response (to MAPKi withdrawal) was transient in some R-lines but persistent in others, suggesting reversible slow-cycling and (by definition, irreversible) cell-death responses, respectively (Fig. 1A). By vital imaging (Fig. 1B), we observed that

Published OnlineFirst September 18, 2017; DOI: 10.1158/2159-8290.CD-17-0682

a subset of R-lines responded to MAPKi withdrawal by slowing down proliferation, whereas a distinct subset responded predominantly by cell death (Fig. 1C). Consistently, cell-cycle slowdown predominant R-lines off-MAPKi displayed relatively lower CFSE dye dilution compared with on-MAPKi (Fig. 1D). On the other hand, residual cells that escaped a predominantly cell-death response to drug withdrawal tended to retain dye strongly relative to the same R-lines on-MAPKi and the slow-cycling R-lines off-MAPKi (Fig. 1D). Furthermore, greater fractions of persisting cells after MAPKi withdrawal displayed senescence-associated β-galactosidase staining in the cell death–predominant R-lines (Fig. 1E), consistent with a reduced proliferative potential. Thus, a cell death–predominant drug-addiction phenotype characterizes MAPKi-resistant melanoma cells that, upon drug withdrawal, undergo cell death in the majority subpopulation and a robust and persistent cell-cycle deceleration in the minority, remainder subpopulation. On the other hand, a slow cycling–predominant drug-addiction phenotype characterizes MAPKi-resistant melanoma cells that, upon drug withdrawal, undergo a transient cell-cycle deceleration (Fig. 1F).

Extent of ERK Rebound Induced by MAPKi Withdrawal Dictates Tumor Cell Slow-Cycling or Death Responses

We then assessed whether the extent of MAPKi withdrawal–induced pERK rebound (fold change from baseline) is causally related to distinct phenotypic outcomes. Cell death–predominant R-lines displayed greater pERK rebound when compared with the slow cycling–predominant R-lines (Supplementary Fig. S1B and S1C). Moreover, a suboptimal or low dose of an ERKi (Supplementary Fig. S1D), when added to cell death–predominant R-lines concomitant with MAPKi withdrawal, completely blocked cell death (Supplementary Fig. S1E) and, when added to both groups of R-lines during MAPKi withdrawal, reversed cell-cycle deceleration (Supplementary Fig. S1F). Consistently, suboptimal ERKi protected all R-lines from clonogenic growth suppression spurred by BRAFi +MEKi (in $BRAF^{MUT}$ R-lines) or MEKi (in $NRAS^{MUT}$ R-lines) withdrawal (Supplementary Fig. S1G). We then tested whether augmenting MAPKi withdrawal–induced pERK rebound in a slow cycling–predominant R-line would enhance MAPKi addiction. $BRAF^{V600E}$ amplification drives acquired MAPKi resistance via ERK reactivation (6) and has been associated with BRAFi (10) or BRAFi + MEKi (2) addiction. We engineered exogenous $BRAF^{V600E}$ overexpression in the slow cycling–predominant R-lines SKMEL28 DDR1 (Supplementary Fig. S1H), which increased pERK levels on and especially off double-drug treatment. Functionally, $BRAF^{V600E}$ overexpression, upon double-drug withdrawal, enhanced cell-death and cell-cycle deceleration, and suppressed long- and short-term growth (Supplementary Fig. S1I–S1L). Hence, the extent of pERK rebound upon MAPKi withdrawal determines the addiction phenotype of MAPKi-resistant melanoma (Supplementary Fig. S1M).

Effectors of Cell-Cycle or Death Responses to MAPKi Withdrawal in Resistant Melanoma

To identify the effectors of distinct MAPKi-addiction phenotypes in drug-resistant melanoma, we generated RNA-sequencing (RNA-seq) profiles of cell death–predominant (M249 DDR5) and slow cycling–predominant (SKMEL28 DDR1) R-lines on (6 hours) or off (6 hours and 24 hours) BRAFi + MEKi. From genes that were induced ≥2 fold by double-drug withdrawal in both R-lines and at both time points (Supplementary Fig. S2A), we analyzed for transcription factor (TF)–binding motif enrichment of the differentially up-expressed genes (Supplementary Fig. S2B). Among the six TFs whose binding motifs were enriched, four (JUNB, FOSL1/FRA1, FOSL2, and c-JUN) belonged to the AP1 family. Among these, *JUNB* and *FOSL1/FRA1* transcripts were induced by MAPKi withdrawal (Supplementary Fig. S2C). At the protein level, both total FRA1 (and pFRA1) and total JUNB were induced by MAPKi withdrawal, together with induction of total FOS (and pFOS), FOSB, and p-p38, the upstream kinase (Supplementary Fig. S2D and see below). In slow cycling–predominant R-lines, double-drug withdrawal induced levels of pFRA1, p-p38, and the cell-cycle inhibitor p21 (Supplementary Fig. S2E). Treatment with a p38 inhibitor (p38i) during MAPKi withdrawal reduced the phosphorylation of its substrate (pHSP27) but not the level of p21. However, treatment with p38i in combination with FRA1 knockdown during MAPKi withdrawal abolished p21 induction, accelerated cell cycling, and reversed 40% to 60% of growth inhibition induced by MAPKi withdrawal in these slow cycling–predominant R-lines (Supplementary Fig. S2E–S2H). Given that JUNB was induced by MAPKi withdrawal (Supplementary Fig. S2C and S2I), we knocked down JUNB. Interestingly, joint JUNB and FRA1 knockdown abolished p21 induction by MAPKi withdrawal and recovered the growth of slow cycling–predominant R-lines after double-drug withdrawal (Supplementary Fig. S2I and S2J). However, sh*FRA1* transduction together with p38i treatment in a cell death–predominant R-line, M249 DDR5, blunted MAPKi withdrawal–induced p21 but failed to alter the cell-cycling profile, likely because the major growth inhibition phenotype, i.e., cell death, was not affected (Supplementary Fig. S2K–S2M). Consistently, M249 DDR5 was still strongly addicted to BRAFi + MEKi despite FRA1 knockdown and p38 inhibition (Supplementary Fig. S2N). Thus, p38–FRA1/JUNB signaling and p21 accumulation induced by MAPKi withdrawal are necessary for the slow cycling but not the cell death–predominant phenotype of drug addiction.

To identify processes that drive the cell death–predominant MAPKi-addiction phenotype, we analyzed the RNA-seq data for differential gene set enrichment between SKMEL28 DDR1 and M249 DDR5 [using the C2 (CGP subset), C6, and hallmark gene sets in MSigDB version 5.1] under each condition (on drug for 6 hours, off drug for 6 hours, off drug for 24 hours). We selected gene sets that showed higher (median $\log_2$ difference of 1.25-fold or 25% up-expression across all genes in the set) gene set enrichment in one R-line compared with the other in either the 6 hours or 24 hours off drug condition, provided that this differential enrichment was higher (by 25%) than that observed in the baseline (on drug for 6 hours) condition. The gene sets that were more strongly enriched in the cell death–predominant R-line (M249 DDR5) off MAPKi for 6 hours or 24 hours are shown in Fig. 2A. As expected, gene sets induced by MAPK hyperactivation were preferentially enriched in the cell death–predominant R-line (M249 DDR5) off double-drugs. Several gene sets induced by DNA damage were also preferentially enriched in M249

Published OnlineFirst September 18, 2017; DOI: 10.1158/2159-8290.CD-17-0682

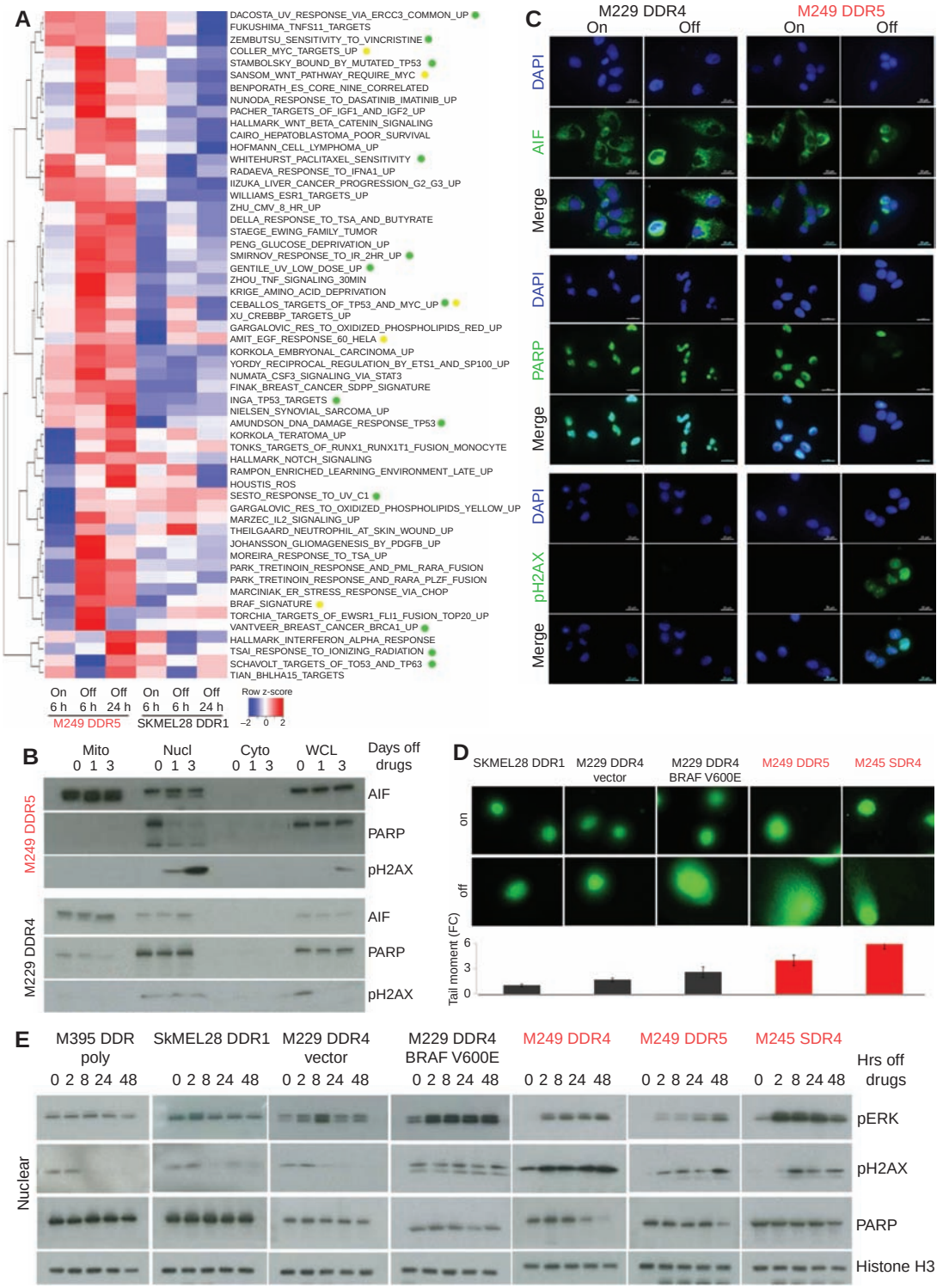

Figure 2. Excessive ERK activation induces DNA damage and AIF-mediated death in the cell death–predominant MAPKi-addiction phenotype. **A,** Heat map showing the gene set variance analysis scores of differentially enriched gene signatures [median log fold change (FC) ≥ 1.25 in the off-drug condition compared with the on-drug condition in either cell line; additionally, differential enrichment between the cell death–predominant and slow cycling–predominant R-lines must also be higher (by at least 25%) in the off-drug condition than in the on-drug condition]. Yellow circles, MAPK hyperactivation gene sets; green circles, DNA damage gene sets. **B** and **C,** Levels of AIF, PARP, and pH2AX measured by Western blots (WB; **B**) or immunofluorescence (IF; **C**) in R-lines on or off MAPKi(s) for 1 and 3 (**B**) or 3 (**C**) days. For **B,** mitochondrial (Mito), nuclear (Nucl), cytoplasmic (Cyto) cellular fractions or whole-cell lysates (WCL). For **C,** nuclei visualized by DAPI; scale bars, 20 μm. **D,** DNA strand break measurements by the comet assay of R-lines on or off MAPKi(s) for 3 days. Tail length/moment FCs were quantified ($n = 5$; mean ± SDs). **E,** Temporal levels of pERK, pH2AX, and PARP in the nuclear fraction of R-cell lysates measured by WBs at indicated hours off MAPKi(s). Histone H3, loading control. (*continued on following page*)

Published OnlineFirst September 18, 2017; DOI: 10.1158/2159-8290.CD-17-0682

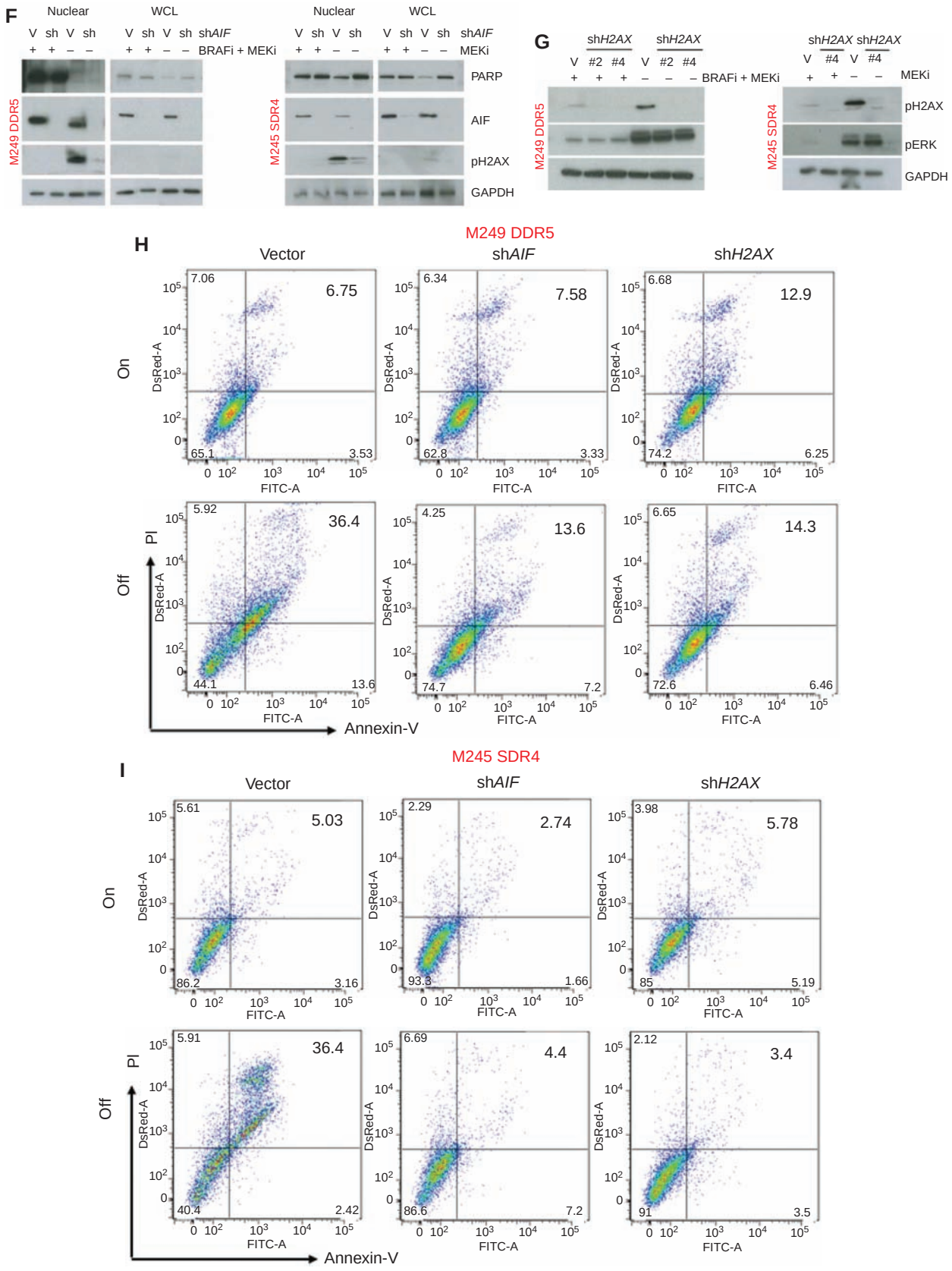

Figure 2. ***(Continued)*** **F** and **G,** Levels of indicated proteins by WBs in the nuclear fraction (**F, G**) or WCL (**F**) of R-lines, on or off MAPKi(s), transduced with empty vector (V) or AIF (**F**) or H2AX (**G**) shRNA lentiviruses. **H–M,** Percentages of Annexin-V/PI-positive dead cells (**H, I**), (*continued on next page*)

Published OnlineFirst September 18, 2017; DOI: 10.1158/2159-8290.CD-17-0682

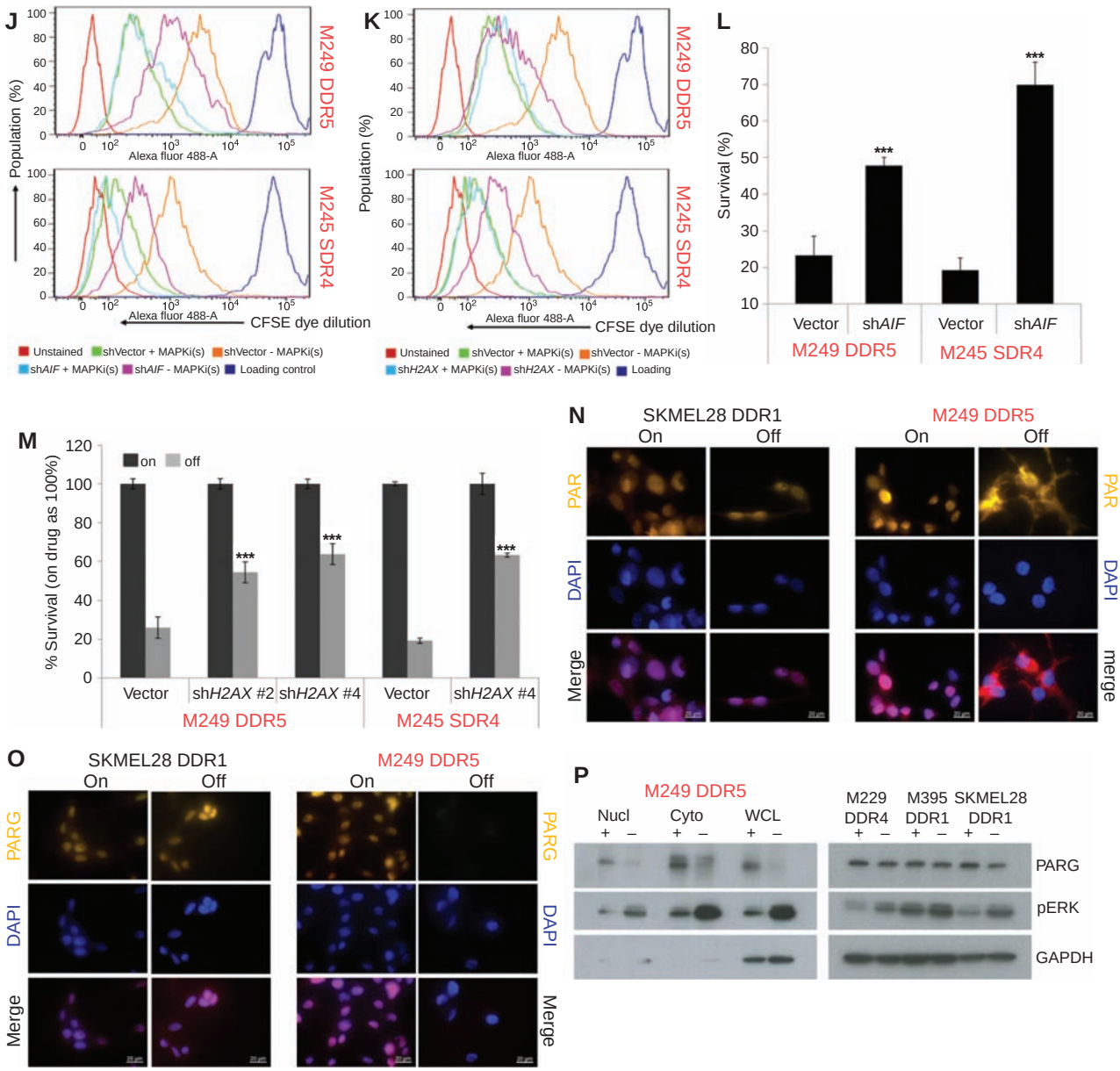

Figure 2. ***(Continued)*** CFSE dye dilution patterns (**J, K**), and viable cell counts (**L, M**) in R-lines on or off MAPKi(s) for 6 days, transduced with empty vector (Vector) or AIF (**J, L**) or H2AX (**K, M**) shRNA lentiviruses. For **L, M,** $n = 6$; mean ± SDs; ***, $P < 0.001$ based on ANOVA. **N** and **O,** Subcellular localization of PAR (**N**) or levels of PARG (**O**) by IF in R-lines. Nuclei visualized by DAPI; scale bars, 20 μm. **P,** PARG and pERK levels by WBs in the indicated fractions of M249 DDR5 or nuclear fractions of indicated additional R-lines. For WB, GAPDH, loading control.

DDR5 when withdrawn from MAPKi. Consistently, when we probed the levels of pH2AX, a marker of DNA damage and mediator of repair, only the cell death–predominant R-line, M249 DDR5, displayed pH2AX induction during MAPKi withdrawal (Fig. 2B and C).

We hypothesized that a strong pERK rebound might induce mitochondrial dysfunction and reactive oxygen species (ROS) and thereby DNA damage. Indeed, MAPKi withdrawal induced pronounced levels of mitochondrial ROS, swelling, and depolarization only in the cell death–predominant R-lines (Supplementary Fig. S3). Pan-caspase inhibition did not rescue cell death–predominant R-lines from cell death or long-term growth inhibition induced by MAPKi withdrawal (Supplementary Fig. S4A and S4B). Consistently, MAPKi withdrawal failed to induce cleaved caspase-3 by measuring its activity or staining (Supplementary Fig. S4C and S4D). We then tested whether AIF, which becomes cleaved and activated by mitochondrial dysfunction or depolarization and nuclear-localized to induce cell death via necrosis or parthanatos (26), might play a role in the cell death–predominant MAPKi-addiction phenotype. Consistently, cleaved AIF accumulated in the nuclear fraction of the cell death–predominant R-line M249 DDR5, but

Published OnlineFirst September 18, 2017; DOI: 10.1158/2159-8290.CD-17-0682

not in the slow cycling–predominant R-line M229 DDR4, after MAPKi withdrawal, in conjunction with nuclear loss of PARP1, a binding partner of AIF and pH2AX (Fig. 2B and C). By using the comet assay, we corroborated increased DNA damage preferentially in the cell death–predominant phenotype (Fig. 2D). In fact, when a slow cycling–predominant R-line (M229 DDR4) was engineered with $BRAF^{V600E}$ overexpression, it then displayed increased DNA damage after MAPKi withdrawal, consistent with transition to a cell death–predominant MAPKi-addiction phenotype (Fig. 2D). Furthermore, pERK rebound coincided temporally with pH2AX induction in cell death–predominant R-lines (Fig. 2E). By manipulating the levels of pERK rebound pharmacologically, we showed that the extent of pERK rebound among cell death–predominant R-lines was strictly associated with the degree of DNA damage, as measured by the comet assay or levels of pH2AX, or with the level of clonogenic growth (Supplementary Fig. S5A–S5E). In fact, pERK and pH2AX levels, quantified by immunofluorescence detection, across all cell death–predominant lines and tumors (see below) were highly correlated (Supplementary Fig. S5F).

To assess the functional contributions of AIF or H2AX to the cell death–predominant drug-addiction phenotype, we engineered M249 DDR5 and M245 SDR4 to express shVector, sh*AIF* or sh*H2AX* (Fig. 2F and G). Importantly, AIF or H2AX knockdown strongly diminished pH2AX accumulation induced by MAPKi withdrawal and abrogated cell death while reducing cell-cycle deceleration and loss of viable cells (Fig. 2F–M). On the other hand, AIF knockdown did not rescue the growth-inhibitory effect of MAPKi withdrawal in slow cycling–predominant R-lines (Supplementary Fig. S6). Consistent with PAR as a key signal underlying excessive DNA damage-PARP-AIF-mediated parthanatos (a recently characterized variant of programmed cell death; ref. 26), we observed PAR cytoplasmic localization as well as loss of PARG, the major enzyme responsible for PAR catabolism, upon MAPKi withdrawal only in the cell death–predominant R-line M249 DDR5, but not the slow cycling–predominant R-line SKMEL28 DDR1 (Fig. 2N–P). Thus, nonapoptotic programmed cell death driven by excessive DNA damage underlies the cell death–predominant MAPKi-addiction phenotype.

Pharmacologic Induction of DNA Damage Promotes Death across All MAPKi-Resistant Cell Lines but Selectively during MAPKi Withdrawal

Because the prior results suggested a synthetic-lethal relationship between excessive pERK level/rebound and DNA damage in the cell death–predominant drug-addiction phenotype, we tested whether enhancing DNA damage via inhibition of DNA damage repair in slow cycling–predominant R-lines would shift the drug-addiction phenotype toward cell death. We treated four slow cycling–predominant R-lines with ATMi, PARPi, or both after MAPKi withdrawal. In SKMEL28 DDR1, M229 DDR4, M238 DDR1, and M395 DDR poly, ATMi + PARPi added upon BRAFi + MEKi withdrawal strongly promoted pH2AX accumulation (Fig. 3A; Supplementary Fig. S7A), suppressed clonogenic growth or cell viability (Fig. 3B; Supplementary Fig. S7B and S7C), and induced cell death 6- to 10-fold (vs. only 2- to 4-fold on MAPKi; Fig. 3C; Supplementary S7D). To confirm the functional importance of DNA damage or its impaired repair in determining the cellular fate (death vs. slow-cycling) of R-lines off MAPKi or during pERK rebound, we knocked down BRCA1 in the slow cycling–predominant R-lines (Supplementary Fig. S7E) and determined the pH2AX levels induced by MAPKi withdrawal, with or without PARPi (Fig. 3D). We found that downregulating DNA damage repair via BRCA1 knockdown and PARP1/2 inhibition, specifically after MAPKi withdrawal, strongly induced DNA damage (pH2AX levels), suppressed clonogenic growth (Fig. 3E) or cell viability (Supplementary Fig. S7F), and induced cell death 4- to 10-fold (vs. 0- to 3-fold on MAPKi; Fig. 3F).

We then assessed whether we could further enhance synthetic lethality in R-lines that were already cell-death predominant in their drug-addiction phenotype. In cell death–predominant R-lines (but not in a slow cycling–predominant R-line), PARPi + ATMi added upon MAPKi withdrawal further induced the nuclear levels of AIF (Fig. 3G). Further boosting the induction of DNA damage (pH2AX levels) and nuclear AIF levels resulted in further clonogenic growth suppression that was evident after prolonged culture off MAPKi (Fig. 3H), consistent with the highest level of cell death detected (early during the course of culture) in cell death–predominant R-lines taken off MAPKi along with PARPi + ATMi cotreatment (Fig. 3I). As earlier data indicated that the cell death–predominant drug-addiction phenotype did not involve induction of caspase-3 activity and could not be reversed by a pan-caspase inhibitor (Supplementary Fig. S4A–S4D), we went further to test whether cell death induced by MAPKi withdrawal plus DNA-damage repair inhibition in slow cycling–predominant R-lines would upregulate caspase-3 activity or function in a caspase-3–dependent manner (Fig. 3J; Supplementary Fig. S4E). As shown clearly, caspase-3 was induced in slow cycling–predominant R-lines specifically during MAPKi withdrawal plus ATMi + PARPi cotreatment but not in a cell death–predominant R-line (Fig. 3K; Supplementary Fig. S4E). Accordingly, in slow cycling–predominant R-lines off MAPKi and on ATMi + PARPi, a caspase-3 inhibitor was able to rescue, at least partially, the drug-resistant melanoma cells from clonogenic suppression (Fig. 3L). In contrast, caspase-3 inhibition, consistent with pan-caspase inhibition (Supplementary Fig. S4A and S4B), failed to reverse the cell death–predominant phenotype (Fig. 3L).

Pharmacologically Augmenting ERK Rebound and DNA Damage Induces Tumor Regression of MEKi-Resistant *NRAS*^{MUT} or Atypical *BRAF*^{MUT} Melanoma

Although MEKi monotherapy has been shown recently to have clinical activity against $NRAS^{MUT}$ melanoma, resistance developed readily (27). Thus, we sought a strategy that would exploit the aforementioned synthetic lethality to augment MEKi addiction in MEKi-resistant $NRAS^{MUT}$ melanoma. Because type I RAF inhibitors, including vemurafenib and dabrafenib, paradoxically activate ERK in the $BRAF^{WT}/NRAS^{MUT}$ context (19–22), we hypothesized that vemurafenib may augment MEKi withdrawal–induced pERK rebound and therefore a cell death–predominant drug-addiction phenotype. To this end, we tested four $NRAS^{MUT}$ melanoma cell lines (from three genetic backgrounds) resistant to

Published OnlineFirst September 18, 2017; DOI: 10.1158/2159-8290.CD-17-0682

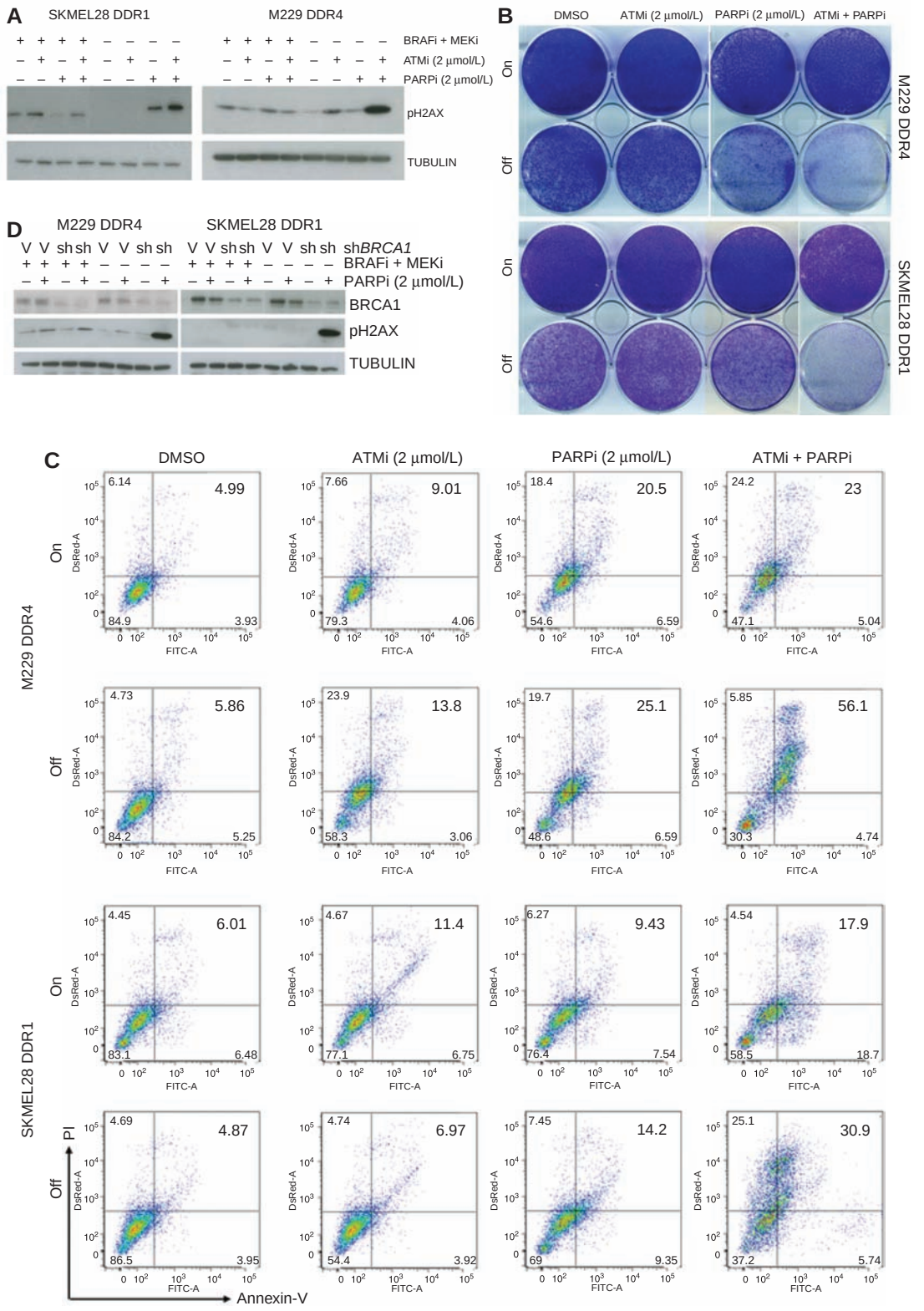

Figure 3. Impairing DNA-damage repair augments MAPKi addiction. **A,** Western blot (WB) analysis of pH2AX levels in slow cycling–predominant R-lines on or off MAPKi(s), with or without ATMi and/or PARPi treatment for 3 days. **B** and **C,** Clonogenic growth (**B**) or percentages of Annexin-V/PI-positive dead cells (**C**) in slow cycling–predominant R-lines on or off MAPKi(s) for 5 days, with or without ATMi and/or PARPi treatment. **D,** WB analysis of BRCA1 and pH2AX levels in slow cycling–predominant R-lines, transduced with empty vector (V) or BRCA1-specific shRNA lentiviruses, on or off MAPKi(s), with or without PARPi treatment for 3 days. (*continued on following page*)

Published OnlineFirst September 18, 2017; DOI: 10.1158/2159-8290.CD-17-0682

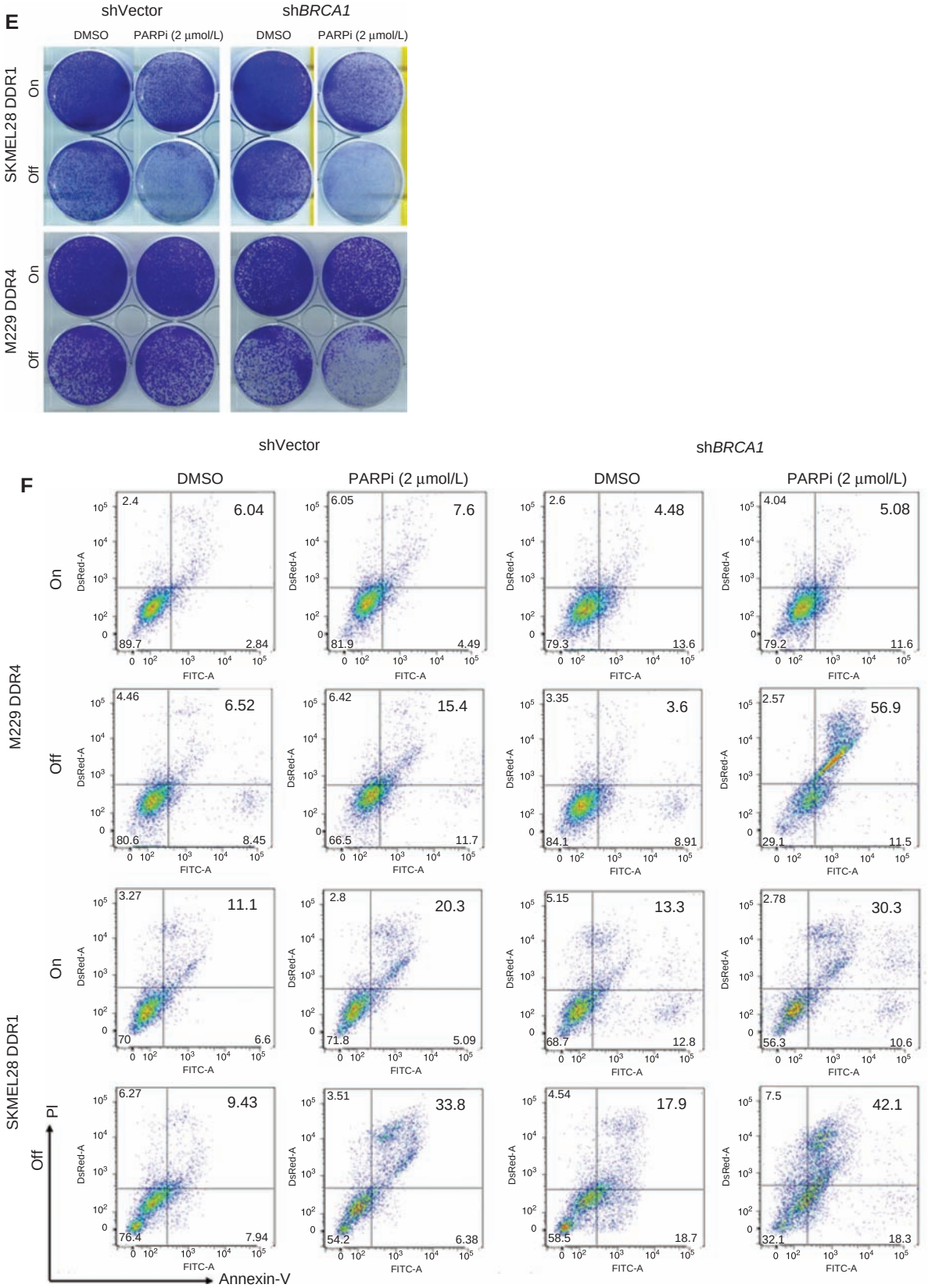

Figure 3. ***(Continued)*** **E** and **F,** R-line cells from **D** were subjected to the same assays as in **B** and **C,** respectively. For WBs, TUBULIN, loading control. (*continued on next page*)

Published OnlineFirst September 18, 2017; DOI: 10.1158/2159-8290.CD-17-0682

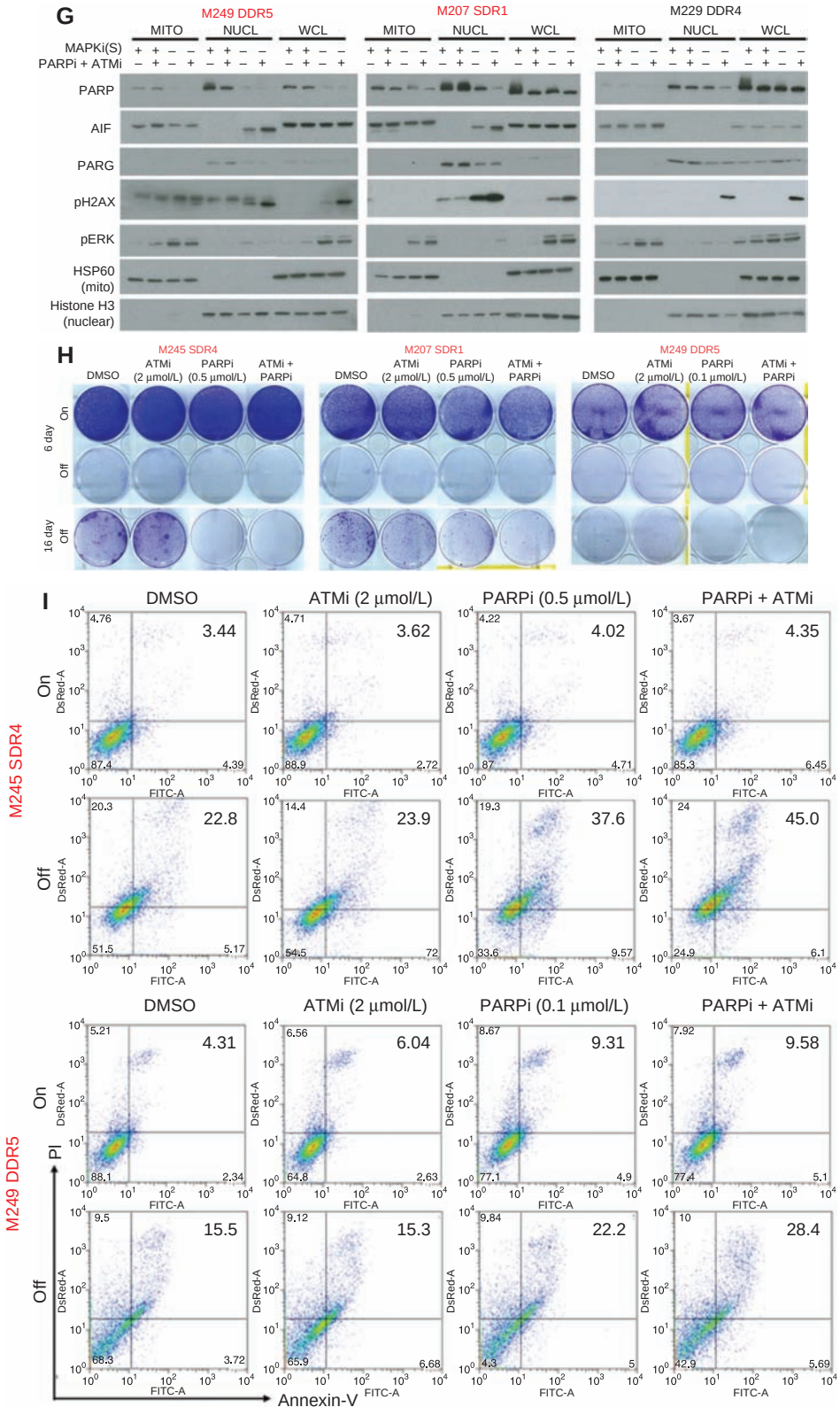

Figure 3. ***(Continued)*** **G,** Levels of indicated proteins by WBs in mitochondrial (MITO), nuclear (NUCL) subcellular fractions or whole-cell lysates (WCL) of slow cycling– versus cell death–predominant R-lines, on or off MAPKi(s), with or without ATMi and PARPi treatment for 3 days. HSP60, mitochondrial fraction control; Histone H3, nuclear fraction control. **H** and **I,** Clonogenic growth (**H**) or percentages of Annexin-V/PI-positive dead cells (**I**) in cell death–predominant R-lines on or off MAPKi(s) for 6 days and 16 days (only in **H**), with or without ATMi and/or PARPi treatment. (*continued on following page*)

Published OnlineFirst September 18, 2017; DOI: 10.1158/2159-8290.CD-17-0682

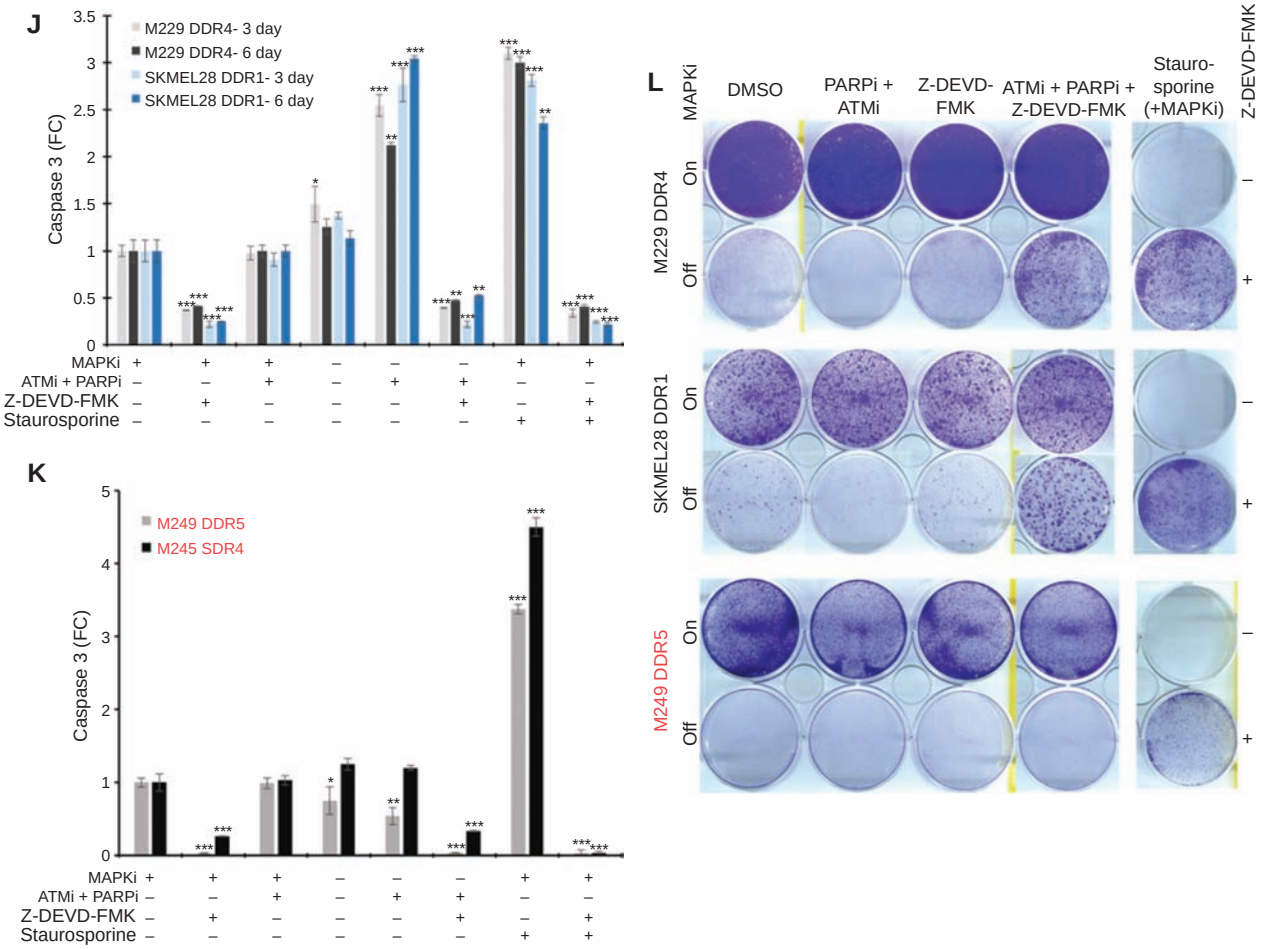

Figure 3. ***(Continued)*** **J–L,** Levels of caspase-3 activity (**J, K**) or clonogenic growth (**L**) with indicated MAPKi(s) treatment, with or without ATMi and PARPi, with or without caspase-3 inhibitor, Z-DEVD-FMK (20 μmol/L), in slow cycling–predominant R-lines (**J**) for 3 or 6 days, or cell death–predominant R-lines (**K**) for 3 days. For **J, K,** $n = 5$; mean ± SDs; *, $P < 0.05$; **, $P < 0.01$; ***, $P < 0.001$ based on ANOVA. Staurosporine (1 μmol/L) used to induce caspase-3 activity and death.

MEKi, which displayed variable degrees of ERK reactivation (on drug) or hyperactivation (off drug; Fig. 4A). Importantly, initiating BRAFi treatment at the time of MEKi withdrawal in these *NRAS*^{MUT} melanoma SDR clones resulted in a more rapid and robust pERK rebound, growth suppression, and cell death, compared with MEKi withdrawal alone (Fig. 4B–D). As was shown with cell death–predominant *BRAF*^{MUT} DDR-lines, MEKi withdrawal with or without BRAFi treatment in these *NRAS*^{MUT} SDR-lines induced pH2AX accumulation and altered PAR and AIF localization (Fig. 4E).

We also tested *in vivo* the synthetic-lethal relationship (between supraphysiologic ERK activity and excessive DNA damage) underlying a cell death–predominant drug-addiction phenotype. We focused on a MEKi-resistant *NRAS*^{MUT} PDX model (Fig. 5A–E) and a MEKi-resistant non-BRAF V600 or atypical *BRAF*-mutant (*BRAF*^{S365L}) PDX model (Fig. 5F–J), because targeted therapies against these melanoma genotypes are currently lacking. To derive a MEKi-resistant *NRAS*^{MUT} PDX model, F1 PDX fragments were transplanted in NSG mice, and mice with tumors of similar volume were treated with trametinib at 5 mg/kg daily (day 25), which led to maximal tumor regression within 10 days (day 33) followed by acquired MEKi resistance (Fig. 5A). One resistant tumor, excised at day 85, was fragmented and serially transplanted into mice with continuous daily MEKi treatment until a cohort of mice with similar tumor volumes was assembled. This group of mice was divided into three subgroups: continuous trametinib, trametinib withdrawal, and vemurafenib treatment with trametinib withdrawal (Fig. 5B). Importantly, withdrawing trametinib (half-life of 4 hours) led to a transient tumor regression. However, vemurafenib treatment upon trametinib withdrawal led to a significantly more sustained tumor regression (Fig. 5B–D). Analysis of these three groups of tumors revealed that, whereas trametinib withdrawal induced pERK, vemurafenib treatment on top of trametinib withdrawal further upregulated pERK (Fig. 5E). Consistent with cell line findings (Fig. 4), trametinib withdrawal, especially with vemurafenib treatment, induced DNA damage or pH2AX (Fig. 5E). Interestingly, trametinib withdrawal plus vemurafenib treatment led to redistribution of nuclear PAR to the cytoplasm (Fig. 5E). Consistent with tumor volumes/sizes/weights, tumors withdrawn from

Published OnlineFirst September 18, 2017; DOI: 10.1158/2159-8290.CD-17-0682

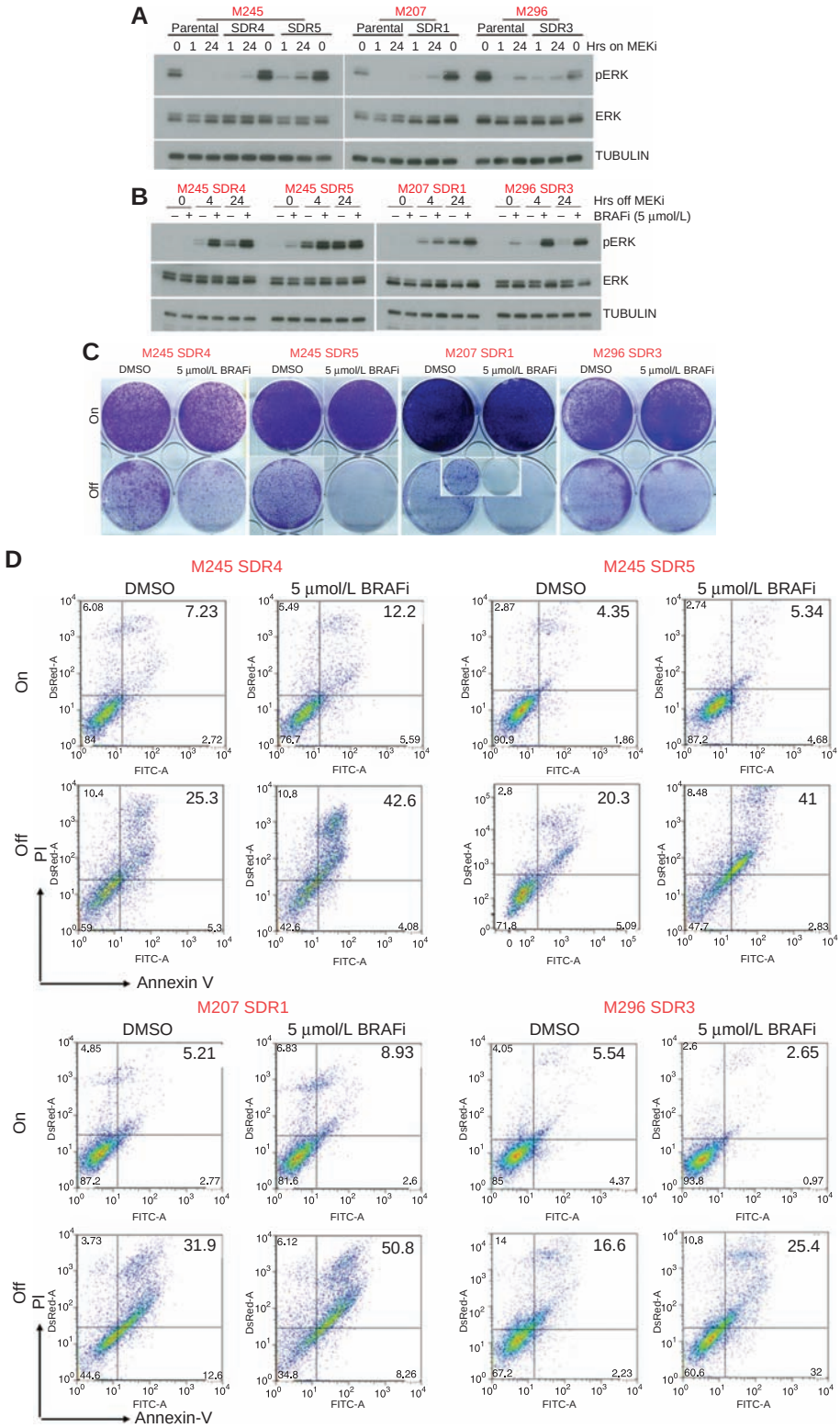

Figure 4. Paradoxical ERK activation by BRAFi potentiates drug addiction in MEKi-resistant *NRAS*^{MUT} melanoma. **A** and **B,** Western blot levels of pERK, ERK, and loading control TUBULIN in *NRAS*^{MUT} parental and isogenic MEKi-resistant SDR-lines with indicated hours on MEKi/trametinib (0.1 μmol/L) treatment (**A**) or in SDR-lines with indicated hours off MEKi/trametinib (0.1 μmol/L) treatment, with or without BRAFi/vemurafenib (5 μmol/L) treatment (**B**). **C** and **D,** Clonogenic growth (**C**) and percentages of Annexin-V/PI-positive dead cells (**D**) in *NRAS*^{MUT} SDR-lines on or off MEKi/trametinib (0.1 μmol/L) for 6 days, with or without BRAFi/vemurafenib (5 μmol/L). Inset for M207 SDR1, off MEKi for 16 days. (*continued on following page*)

Published OnlineFirst September 18, 2017; DOI: 10.1158/2159-8290.CD-17-0682

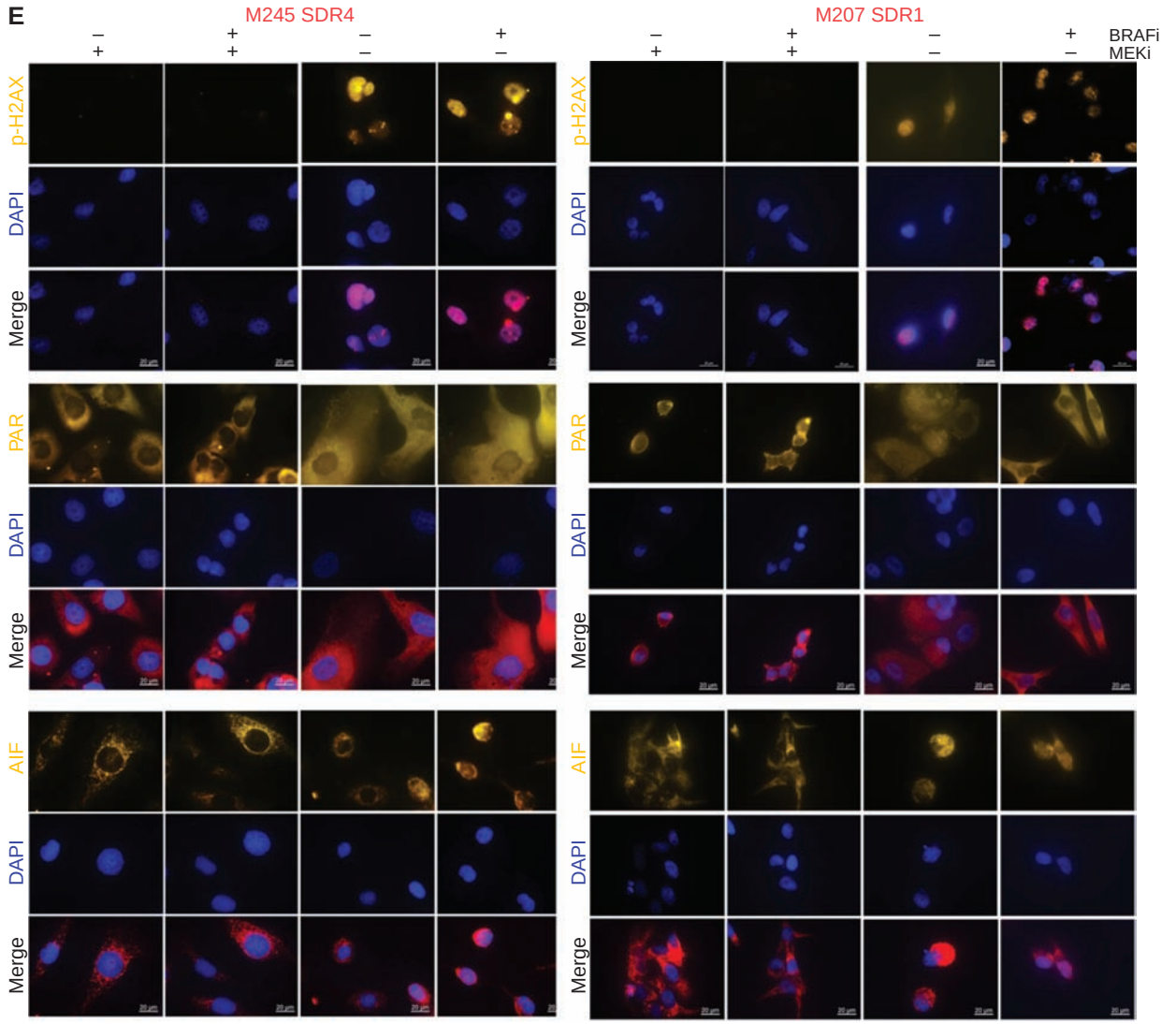

Figure 4. ***(Continued)*** **E,** Levels and/or subcellular localization of pH2AX, PAR, and AIF in cell death–predominant MEKi-addicted R-lines on or off MEKi for 3 days, with or without BRAFi (5 μmol/L) treatment.

trametinib and then treated with vemurafenib displayed the lowest proliferation or Ki67 level (Fig. 5E). To derive a MEKi-resistant atypical *BRAF*^{MUT} PDX model, we treated F1 PDX *BRAF*^{S365L} melanoma tumors in NSG mice with trametinib at 5 mg/kg daily (day 25), which led to maximal tumor regression within 20 days (day 45) followed by acquired MEKi resistance (Fig. 5F). The fastest growing MEKi-resistant tumor was selected for serial transplantation on continuous MEKi therapy and divided into three experimental groups: continuous trametinib, trametinib withdrawal, and vemurafenib treatment with trametinib withdrawal. As with MEKi-resistant *NRAS*^{MUT} PDX tumors, *BRAF*^{S365L} PDX tumors resistant to MEKi responded to MEKi withdrawal but more robustly when a type I RAF inhibitor (vemurafenib) was added during MEKi withdrawal (Fig. 5G–I). Consistent with the notions that non-V600E BRAF mutants operate as RAF dimers and that enhanced RAF dimerization can drive MAPK reactivation and hence acquired MEKi resistance (18), we observed that BRAFi addition during MEKi withdrawal robustly upregulated the pERK level (along with levels of pH2AX, PAR) coincident with Ki67 downregulation (Fig. 5J and Supplementary Fig. S8A).

We then tested whether we could effect deeper and more sustained tumor regression by triggering DNA damage during pERK rebound (Fig. 5K). We noticed *in vitro* (in *NRAS*^{MUT} SDR-lines) that PARPi treatment alone (without ATMi) could enhance to some extent clonogenic suppression and cell death induced by MEKi withdrawal (Fig. 3H and I). Similarly, in long-term clonogenic assays (Supplementary Fig. S8B), although BRAFi or PARPi each could further suppress the growth of *NRAS*^{MUT} SDR-lines withdrawn from MEKi, their combination led to the most profound suppression of growth. Importantly, *in vivo*, MEKi withdrawal combined with BRAFi + PARPi led to the most profound and sustained regression of MEKi-resistant *NRAS*^{MUT} melanoma (Fig. 5K and L), which was associated with the strongest induction

Published OnlineFirst September 18, 2017; DOI: 10.1158/2159-8290.CD-17-0682

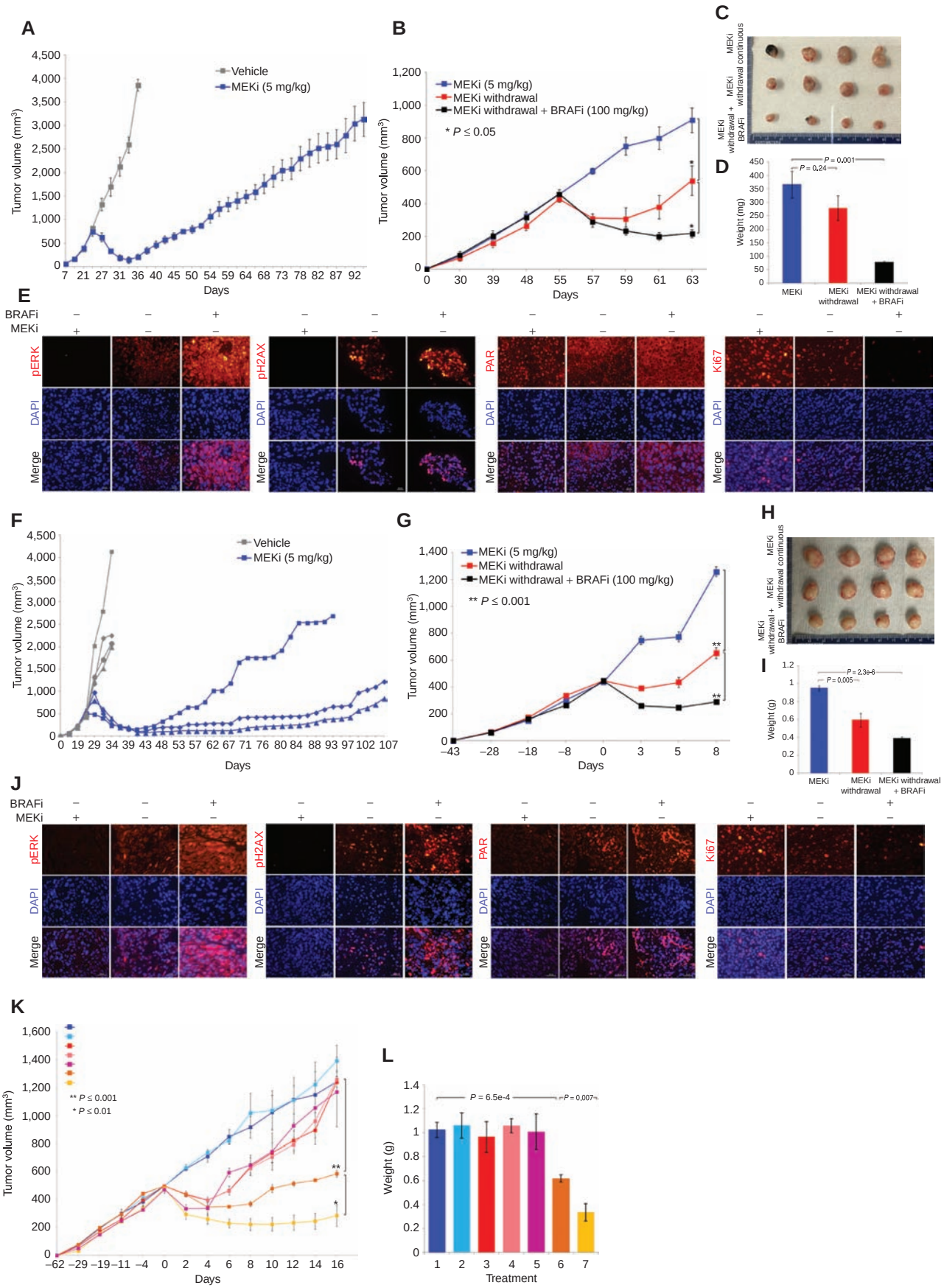

Published OnlineFirst September 18, 2017; DOI: 10.1158/2159-8290.CD-17-0682

of pERK, pH2AX, and PAR and suppression of Ki67 (Supplementary Fig. S8C and S8D). These and additional results (Supplementary Fig. S8E and S8F) suggest that inhibition of PARP specifically (or DNA damage repair in general) may be a potential strategy to augment MAPKi addiction.

We also assessed whether the synthetic lethality (between supraphysiologic levels of activated ERK and DNA damage) observed across MAPKi-resistant human melanoma cell lines and PDX tumors could also be observed in an immune-competent context. To do this, we generated a syngeneic and transplantable model of MEKi-resistant *Nras*^{MUT} melanoma. First, we derived a *Nras*^{Q61R}*/Ink4a/Lkb1* murine melanoma cell line (TpLN^{61R} for Tyrosinase p16 Lkb1 Nras^{Q61R}) from a tumor of the Tyr-CRE-NRAS Q61R genetically engineered murine melanoma model (28) and adapted TpLN^{61R} to efficient *in vivo* subcutaneous growth in C57BL/6 mice. These tumors were then chronically treated with trametinib at 5 mg/kg daily until MEKi-resistant tumors arose (Fig. 6A). We then dissociated a resistant tumor and cultured the tumor cells with trametinib *in vitro* (up to 0.1 μmol/L over three weeks). *In vitro*, this MEKi-resistant cell line, termed NILR2R (Nras, Ink4a, Lkb1, Resistant mouse 2 Right flank), displayed robust time-dependent induction of pERK levels by MEKi withdrawal, which was accelerated by BRAFi treatment (Fig. 6B). Consistent with robust pERK rebound levels, pH2AX was induced by MEKi withdrawal and further induced by BRAFi treatment during MEKi withdrawal (Fig. 6C). Importantly, PARPi treatment (at a low concentration effective in augmenting cell killing among cell death–predominant R-lines, Fig. 3) during MEKi withdrawal and BRAFi treatment resulted in even greater pH2AX accumulation (Fig. 6C). Consistently, although BRAFi and/or PARPi had no appreciable effects on clonogenic growth or cell death levels of NILR2R in the presence of MEKi, BRAFi or PARPi treatment during MEKi withdrawal reduced clonogenic growth and increased the levels of cell death (Fig. 6D and E). Cotreatment of BRAFi and PARPi during MEKi withdrawal further reduced growth and increased death (Fig. 6D and E). Consistent with a cell death–predominant drug-addiction phenotype observed among MAPKi-resistant human melanoma cell lines and PDX tumors, this MEKi-resistant murine melanoma cell line also displayed upregulation of PAR levels and nuclear localization of AIF during induction of the drug-addiction phenotype (Fig. 6F). Finally, we reimplanted NILR2R back into C57BL/6 mice treated with trametinib (5 mg/kg via daily gavage) and identified five groups of mice with closely matched tumor volumes (Fig. 6G). We then tested the individual tumor-shrinkage effect of BRAFi or the combined effect of BRAFi + PARPi treatments *in vivo*. As expected based on prior results, PARPi intraperitoneal treatments had no significant effect on the growth of NILR2R tumors on continuous MEKi oral treatments. MEKi discontinuation alone led to transient tumor shrinkage. Importantly, BRAFi oral treatment beginning with MEKi discontinuation prolonged the tumor-shrinkage effect of MEKi withdrawal (Fig. 6 G–I). PARPi + BRAFi cotreatment during MEKi withdrawal led to the most sustained tumor regression (Fig. 6G). Thus, pharmacologically augmenting ERK rebound and DNA damage to maximize regression of MEKi-resistant *Nras*^{MUT} melanoma tumors during MEKi withdrawal may be feasible in an immune competent host.

DISCUSSION

Understanding the mechanisms underlying the cancer vulnerability of MAPKi addiction availed us with potential therapeutic opportunities (Fig. 7). During a predominantly tumor cell–death rather than cell-cycle deceleration response upon drug withdrawal, MAPKi-resistant melanoma, regardless of the specific underlying driver(s) of resistance, displays a synthetic lethality between acute, suprabasal ERK hyperactivation and excessive DNA damage. Death by this synthetic lethality in the context of a robust pERK rebound is characterized by AIF-dependent but caspase-3–independent death. Impairing DNA-damage repair pharmacologically, on top of DNA damage already induced by strong pERK rebounds, further boosted AIF-dependent death of MAPKi-resistant melanoma cells. On the other hand, a weak MAPKi withdrawal–induced pERK rebound was sufficient to elicit only a cell-cycle slowdown, leading to persisters that will resume rapid proliferation. However, upon MAPKi withdrawal, an innately weak pERK rebound coupled with impairment of the DNA-damage repair machinery turned a predominantly slow-cycling response to a cell-death response that was caspase-3–dependent. Based on these findings, one would expect an even stronger synthetic lethality for drug-withdrawn, MAPKi-resistant melanoma harboring genetic loss of *BRCA1/2* or displaying *BRCA*ness (ref. 29; either preexisting or acquired during MAPKi therapy). Thus, after emergence of MAPKi-resistant clones, targeting the DNA-damage repair pathways subsequent to cessation of MAPKi dosing may specifically select against disease progression across the spectrum of MAPKi-addiction phenotypes.

In the particular contexts of MEKi-resistant *NRAS*^{MUT} melanoma, type I RAF inhibitors such as vemurafenib further augmented ERK rebound (on top of what was induced by MEKi withdrawal) and cell death. Counter to the dogma that type I RAF inhibitor is contraindicated for *NRAS*^{MUT} melanoma, its ability to boost ERK levels in the context of MEKi

Figure 5. Excessive ERK and DNA damage induce regression of MEKi-resistant PDX tumors. **A,** Tumor volumes (mean ± SEM) of a *NRAS*^{MUT} PDX transplanted in NSG mice in response to daily gavage with the vehicle ($n = 3$) or trametinib (5 mg/kg; $n = 5$). **B,** R1 trametinib-resistant *NRAS*^{MUT} PDX tumors were grown in NSG mice for 55 days with daily trametinib (5 mg/kg) gavage until initiating indicated daily treatments or regimens ($n = 4$ in each group). Tumor volumes are shown as means ± SEM. *P* values, Student *t* test. MEKi, trametinib (5 mg/kg); BRAFi, vemurafenib (100 mg/kg). **C,** Pictures of tumors from three experimental groups in **B** on day 63. **D,** Tumor weights (means ± SEM; *P* value, unpaired *t* test) of three experimental groups in **B**. **E,** Levels of indicated proteins in representative tissue sections of tumors in **C**. Scale bars, 20 μm. **F–J,** As in **A** to **E** except experiments used a distinct PDX model harboring *BRAF*^{S365L} and individual tumor growth curves were plotted separately in **F**. The MEKi-resistant tumor (R3) which arose first was fragmented, serially passaged, and used in **G**. **K** and **L,** R1 trametinib-resistant *NRAS*^{MUT} PDX tumors were serially passaged in NSG mice with daily trametinib (5 mg/kg) gavage until segregation into seven groups (1, 2, 3, 5, $n = 3$ per group; 4, 6, 7, $n = 5$ per group). Tumor volumes and weights are shown as means ± SEM. *P* values, Student *t* test.

Published OnlineFirst September 18, 2017; DOI: 10.1158/2159-8290.CD-17-0682

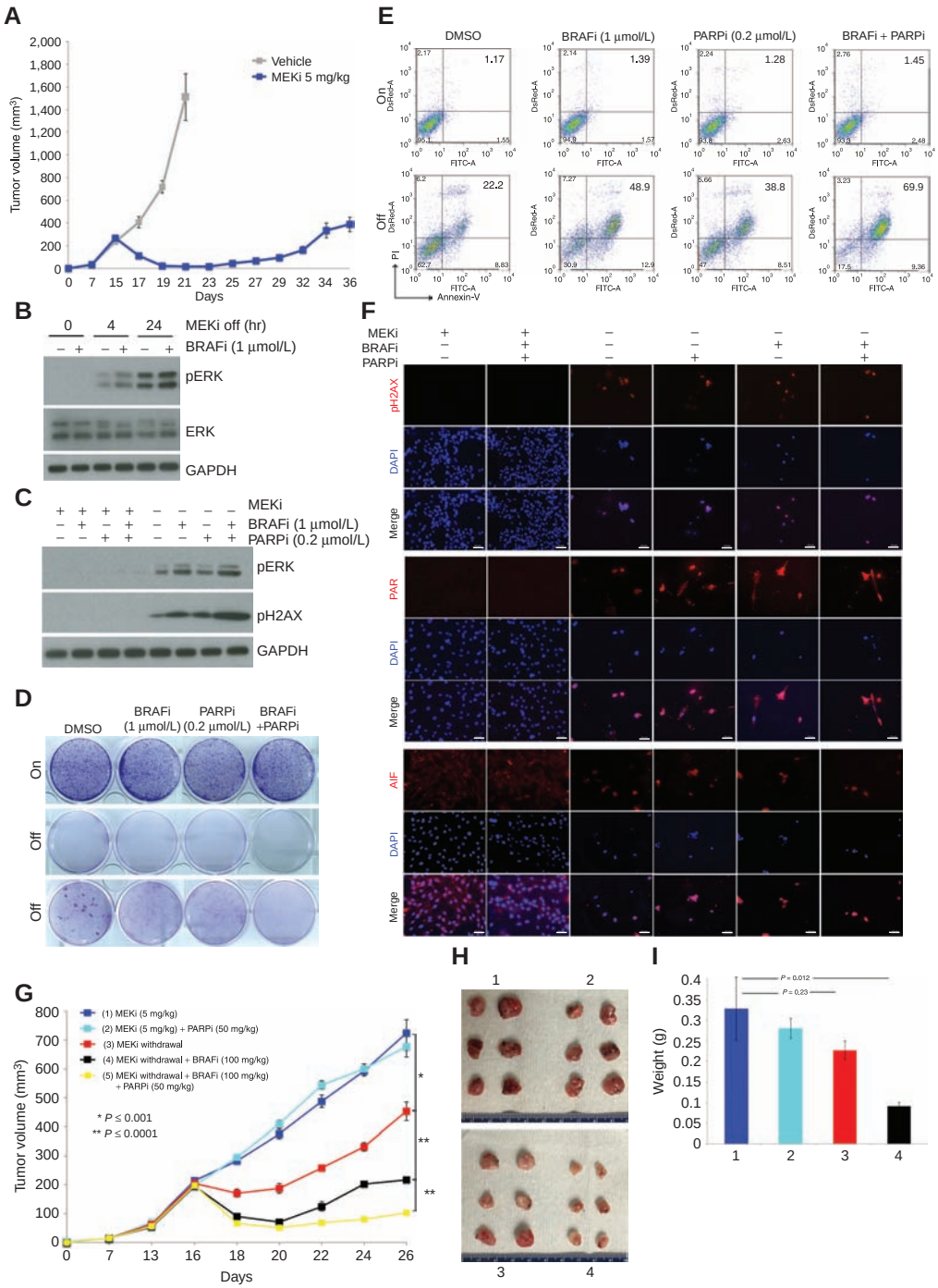

Figure 6. BRAF and PARP inhibitors augment MEKi addiction of *Nras*^{MUT} murine melanoma in an immune competent host. **A,** Tumor volumes (mean ± SEM) of TpLN^{61R} murine melanoma cells transplanted in C57BL/6 mice in response to daily gavage with the vehicle ($n = 6$) or trametinib (5 mg/kg; $n = 6$). One resistant tumor on day 36 was dissociated and cultured as a MEKi-resistant cell line (NILR2R). **B,** Western blot levels of pERK, ERK, and the loading control GAPDH in the MEKi-resistant *Nras*^{MUT} SDR-line NILR2R, with indicated hours off MEKi/trametinib (0.1 μmol/L) treatment, with or without BRAFi/vemurafenib (1 μmol/L) treatment. **C,** Analysis of NILR2R protein lysates by Western blots of pERK and pH2AX levels on or off MEKi, with or without BRAFi (1μmol/L) and/or PARPi (0.2 μmol/L) treatment for 3 days. **D** and **E,** Clonogenic growth (**D**; 8 days) and percentages of Annexin-V/PI-positive dead cells (**E**; 5 days) in NILR2R, on or off MEKi/trametinib (0.1 μmol/L), with or without BRAFi/vemurafenib (1 μmol/L) and/or PARPi (0.2 μmol/L) treatments. For **D,** cultures were seeded at 30K cells per well, except for the third row where cultures were seeded at 150K cells per well. **F,** Levels and/or subcellular localization of pH2AX, PAR, and AIF in NILR2R, on or off MEKi for 3 days, with or without BRAFi and/or PARPi treatment. Scale bars, 20 μm. **G,** Trametinib-resistant NILR2R cells were transplanted subcutaneously in C57BL/6 mice with daily trametinib (5 mg/kg) gavage until segregation into five groups ($n = 6$ per group). Tumor volumes are shown as means ± SEM. *P* values, Student *t* test. **H,** Pictures of tumors from the first four experimental groups (mice sacrificed due to tumor ulceration) in **G** on day 26. **I,** Tumor weights (means ± SEM; *P* value, unpaired two-way *t* test) of the first four experimental groups in **G**.

Published OnlineFirst September 18, 2017; DOI: 10.1158/2159-8290.CD-17-0682

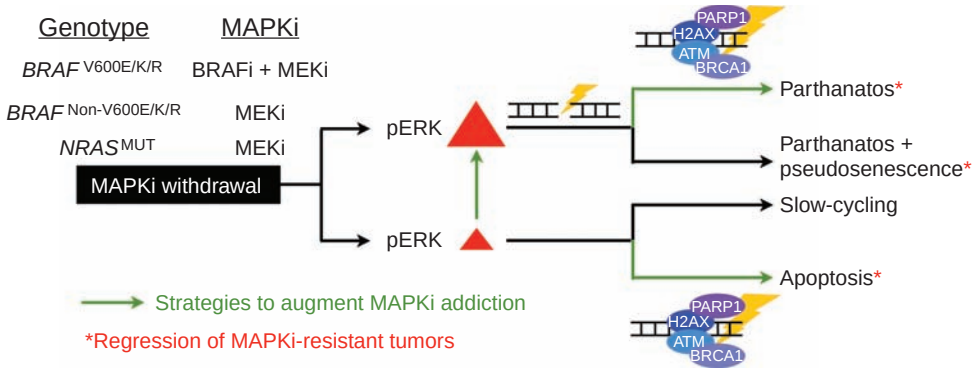

Figure 7. Strategies to select against MAPKi-resistant melanoma. Schematic showing MAPKi-addiction phenotypes being driven by pERK rebound levels and potential therapeutic strategies (enhancing pERK or impairing DNA-damage repair) that promote tumor cell death (apoptosis or parthanatos) or regression.

addiction suggests a novel context-dependent application. Furthermore, MEKi-resistant melanoma with atypical *BRAF*^{MUT} mutations likely upregulated RAF dimer levels (as a mechanism of resistance). This may explain the ability of vemurafenib to enhance pERK induction and tumor regression during MEKi withdrawal. Given the potential liability of prolonged BRAFi treatment in these genetic contexts, further studies are required to define an optimal BRAFi treatment duration in the context of augmenting drug addiction.

This study highlights the potential utility of capitalizing on MAPKi-addiction mechanisms to control MAPKi-resistant subclones even before the development of clinically evident disease progression. Our recent study identified melanoma tumors, during MAPKi-induced regression, to be undergoing dynamic and stereotypic tumor cell and immune compartmental adaptations (30). It will also be important to characterize the immune infiltration/composition and identify specific adaptive immune resistance mechanisms associated with tumor regression resulting from a pharmacologically augmented drug-addiction phenotype. Furthermore, MAPK inhibitors with ideal clinical pharmacokinetic properties (short half-lives, e.g., encorafenib, binimetinib) may be particularly useful for implementation of strategies based on MAPKi addiction in human subjects. Finally, understanding in further detail how excessive ERK and DNA damage levels engage distinct programmed cell death pathways promises to guide the development of rotational therapies that adapt to evolving cancer vulnerabilities.

METHODS

Cell Culture, Subline Derivation, Constructs, and Inhibitors

All cell lines were routinely tested for *Mycoplasma*, and cell line and subline identities have been ensured by the GenePrint 10 system (Promega) at routine intervals during the course of this study for banking and experimental studies. All cell lines were maintained in DMEM high glucose with 10% heat-inactivated FBS (Omega Scientific) and 2 mmol/L glutamine in a humidified, 5% CO_2 incubator. All M series cell lines were established from patient-derived tumors at the University of California, Los Angeles (UCLA). The TpLN^{61R} cell line was derived at the University of North Carolina and adapted to *in vivo* growth at UCLA in 2016. The NILR2R cell line was established *in vitro* from a MEKi-resistant tumor at UCLA in 2017. SKMEL28 was obtained from Dr. Alan Houghton (between 2008 and 2010). To derive resistant clones, parental melanoma cells seeded at low density were treated with BRAFi + MEKi (vemurafenib + selumetinib; *BRAF*^{MUT}) or MEKi (trametinib; *NRAS*^{MUT}) every 2 to 3 days for 6 to 12 weeks, and proliferative colonies were ring-isolated (except those designated "poly" for polyclonal where ring cloning was not performed) and expanded. sh*H2AX*, sh*FRA1*, sh*JUNB*, and vector (pLKO.1) were obtained commercially (ThermoFisher). sh*BRCA1* and vector (pGIPZ) were accessed through the Molecular Screening Shared Resource at UCLA. *BRAF*^{V600E} was subcloned into the doxycycline-repressible lentiviral vector pLVX-Tight-Puro (ClontechLaboratories). Overexpression and knockdown constructs were packaged into lentiviral particles for infection. Inhibitors were obtained from the following: vemurafenib *in vitro* (Plexxikon); vemurafenib *in vivo*, selumetinib *in vitro*, trametinib *in vitro* and *in vivo* (LC Laboratories); ERKi/SCH772984 (Merck); p38i/SB203580, PARPi/Olaparib, ATMi/KU-55933, and caspasei/Z-VAD-FMK (Selleckchem).

Protein Detection

Cells were lysed in RIPA buffer (Sigma) with protease inhibitor (Roche) and phosphatase inhibitor (Santa Cruz Biotechnology) cocktails for Western blotting. For immunohistochemistry (IHC), tissues were fixed either in 4% paraformaldehyde (PFA) and sucrose cryoprotected in OCT or in formalin and embedded in paraffin (FFPE). For FFPE tissues, after deparaffinization and rehydration, tissue sections were subjected heat for antigen retrieval. PFA/OCT sections were not subjected to antigen retrieval. Both IHC and immunocytochemistry of cell lines were performed with Alexa Fluor–conjugated secondary antibodies (Life Technologies) on 4% PFA-fixed cells. Nuclei were counterstained by DAPI. Fluorophore signals were captured with a Zeiss microscope (AXIO Imager A1) mounted with a charge-coupled device camera (Retiga EXi QImaging), and the images captured by Image-pro plus 6.0. Western blots and immunofluorescence assays were performed using the following antibodies: pERK1/2 (T202/Y204), p-c-FOS (S32), pFRA1 (S265), p-p38 MAPK (T180/Y182), p-HSP27 (S82), pHistone H2A.X (S139), total ERK1/2, c-FOS, FRA1, FOSB, p21, AIF, PARG, BRCA1, GAPDH (Cell Signaling Technology), TUBULIN (Sigma), PARP1, BRAF (Santa Cruz Biotechnology), PAR (Enzo), and Ki67 (EMD Millipore). Western blot quantification was performed using NIH ImageJ.

Cell Line–Based Assays

Clonogenic assays were performed by plating cells at single-cell density in six-well plates, and inhibitor/media replenished every 2 days for 7 days, unless noted otherwise. Colonies were fixed in 4% paraformaldehyde and stained with 0.05% crystal violet. Viable cell

Published OnlineFirst September 18, 2017; DOI: 10.1158/2159-8290.CD-17-0682

counts were performed in triplicate wells (in six-well plates). Cell death assays were performed by plating indicated cell lines with or without MAPKi(s) for 6 days (unless otherwise indicated), and cells were stained with Annexin V–FITC and propidium iodide for 15 minutes at room temperature before sample loading (LSR II Flow Cytometry, BD Bioscience). CFSE (Molecular Probes) dilution detected by flow cytometry was used to monitor cell division. Cells were loaded with 3 μmol/L of CFSE and cultured for 6 days. Samples were collected and fixed in 2% PFA and analyzed with LSRII. Flow cytometry data were analyzed by FlowJo. Senescence was assessed by a Senescence Associated β-Galactosidase staining kit (Cell Signaling Technology) with MAPKi withdrawn for 6 days. For vital imaging, cells were plated onto gridded dishes (Sigma) and imaged at indicated time points at predesignated areas. Comet assays (Cell Biolabs, Inc.) were performed by plating cell lines in six-well plates in the presence or absence of MAPKi for 3 days. Stranded breaks were detected by following the manufacturer's recommendations, imaged with a Zeiss microscope (AXIO Imager A1), and distance of tails measured with Image-pro plus 6.0. Caspase-3 activity was assessed using Caspase-Glo 3/7 kit (Promega) by plating cells in white-walled, 96-well plates in the presence or absence of indicated inhibitors for 3 or 6 days.

RNA-seq Analysis

RNA-seq data from cell lines were generated using 2 × 100 bp paired-end sequencing using the Illumina HiSeq2000 platform. Paired-end reads were mapped to the UCSC hg19 reference genome using Tophat2 (31). Normalized expression levels of genes were expressed in FPKM values as generated by cuffquant and cuffnorm. Both programs were run with the option "–frag-bias-correct" and "–multi-read-correct" to improve sensitivity. For differential gene expression calls, a gene was defined as differentially expressed when its expression increased or decreased by at least 2-fold. RNA-seq runs on multiple sequencing lanes were independently mapped, and the expression values of each gene (in FPKM) were averaged across multiple lanes. To overcome noise in differential expression values caused by extremely low FPKM levels, we added a pseudo-FPKM value of 0.1 to all expression values. RNA-seq data have been made available through the Gene Expression Omnibus (GEO) at the accession number GSE87326.

Transcription Factor Enrichment Analysis

We collected transcription factor (TF) binding motifs in the form of position weight matrices (PWM) from the JASPAR database (32). Instead of using a fixed PWM score cutoff(s) as done in other PWM matching programs, we estimated the significance of the PWM score in a gene's promoter, which is defined as −1,500 to +1,500 bp from transcription start site (TSS), by comparing the score with a background distribution of the same PWM's scores on nonpromoter regions from randomly selected genes. Specifically, we collected 10,000 random 3 KB intragenic regions (excluding the genes' promoter regions) and, for each sequence, computed the best score of a PWM. These scores defined an empirical background distribution of the PWM, and we defined a significant match of the PWM if and only if (i) the PWM score was greater than or equal to the 95th percentile of the background PWM scores (i.e., $P \leq 0.05$) and (ii) a PWM score was at least 0.75. This approach avoided applying the same absolute PWM score cutoff on PWMs with differing lengths and complexities. To estimate enrichment of a TF's PWM W in a set of coregulated genes G, we compared the number of significant matches of W in the promoter regions in G (accounting for possible multiple TSS for each gene) and the number of matches against a set of randomly selected promoter regions of the same size. We repeated the latter step 100,000 times to estimate the empirical enrichment *P* value of the PWM. Finally, we corrected the PWM enrichment *P* values across all tested PWMs for multiple hypothesis testing using the Benjamini–Hochberg (FDR) method. A TF's PWM was defined as enriched in a set of genes when its adjusted enrichment *P* value was ≤ 0.05.

Gene Set Enrichment Analysis

Paired gene set enrichment analyses between off- versus on-drug conditions or between two different cell lines were performed as described previously (1). We computed differential gene set enrichments of the gene sets in the C2 CGP, C6, and Hallmark subsets from the Molecular Signature Database of the Broad Institute using the following steps: (i) We calculated $\log_2$ fold changes ($\log_2$ FC) of mRNA expression of each gene in M249 DDR5 compared with SKMEL28 DDR1 at all three treatment conditions, i.e., on-drug 6 hours, off-drug 6 and 24 hours; (ii) Based on the $\log_2$ FC values, we computed the differential enrichment of each gene set between M249 DDR5 and SKMEL28 DDR1 in all three treatment conditions (cutoff for differential enrichment, Wilcoxon rank-sum test between genes within the gene set and the rest of the genes; $P \leq 0.05$; median of up-expression across all genes in the gene set ≥ 25%, i.e., median $\log_2$ FC ≥ 0.322); (iii) To exclude differential enrichment already present between on-drug condition, for each of the gene sets meeting the cutoffs in step 2, we required that the difference between the median $\log_2$ FC in either off-drug condition to be higher than the median $\log_2$ FC in the on-drug condition by at least 0.322 (1.25-fold higher); and (iv) For visualization, we computed the single sample enrichment GSVA scores (33) of the selected gene sets from step 3 using $\log_2$ CPM values as input.

PDX Models and Murine Melanoma

Mouse experiments were approved by the Animal Research Committee at UCLA. Tumor fragments derived from a $NRAS^{Q61R}$ and a $BRAF^{S365L}$ metastatic melanoma (F0), which were obtained from two distinct patients with approval by the local Institutional Review Board, were transplanted subcutaneously in sex-matched NSG mice (6–8 weeks old). Tumors were measured with a caliper every 2 days, and tumor volumes were calculated using the formula (length × width^2)/2. Trametinib-resistant tumors were cut into fragments, which were serially transplanted. NILR2R cells were injected at 1 million cells per flank in C57BL/6 mice. Mice were treated with vehicle (0.5% HPMC–0.2% Tween 80, pH8), trametinib (5 mg/kg), or vemurafenib (100 mg/kg) by oral gavage daily, or olaparib (25 or 50 mg/kg) by daily i.p. injections.

Disclosure of Potential Conflicts of Interest

N.E. Sharpless has ownership interest (including patents) in G1 Therapeutics and is a consultant/advisory board member for the same. No potential conflicts of interest were disclosed by the other authors.

Authors' Contributions

Conception and design: A. Hong, G. Moriceau, S. Lomeli, R.S. Lo
Development of methodology: A. Hong, G. Moriceau, S. Lomeli, R. Damoiseaux, W. Hugo, R.S. Lo
Acquisition of data (provided animals, acquired and managed patients, provided facilities, etc.): A. Hong, G. Moriceau, M. Piva, R. Damoiseaux, S.L. Holmen, N.E. Sharpless, R.S. Lo
Analysis and interpretation of data (e.g., statistical analysis, biostatistics, computational analysis): A. Hong, G. Moriceau, L. Sun, S. Lomeli, M. Piva, N.E. Sharpless, W. Hugo, R.S. Lo
Writing, review, and/or revision of the manuscript: A. Hong, G. Moriceau, L. Sun, S. Lomeli, M. Piva, N.E. Sharpless, W. Hugo, R.S. Lo
Administrative, technical, or material support (i.e., reporting or organizing data, constructing databases): A. Hong, L. Sun, W. Hugo, R.S. Lo
Study supervision: R.S. Lo

Acknowledgments

We thank G. Bollag (Plexxikon Inc.) for providing PLX4032, and S. Hu-Lieskovan (UCLA), J. Zaretsky (UCLA), P.J. Kaplan-Lefko (UCLA), and A. Ribas (UCLA) for assisting with animal work.

Grant Support

This work has been funded by Burroughs Wellcome Fund (to R.S. Lo), the National Institutes of Health (1R01CA176111 and P01CA168585 to R.S. Lo), the Ressler Family Foundation (to R.S. Lo), the Melanoma Research Alliance (to R.S. Lo and W. Hugo), the Ian Copeland Melanoma Fund (to R.S. Lo), the SWOG/Hope Foundation (to R.S. Lo), the Steven C. Gordon Family Foundation (to R.S. Lo), the Melanoma Research Foundation (to R.S. Lo), the American Skin Association (to W. Hugo), the American Association for Cancer Research-Amgen, Inc. Fellowship in Clinical/Translational Cancer Research (16-40-11-HUGO to W. Hugo), the Department of Defense Horizon Award (to A. Hong), and the Dermatology Foundation (to G. Moriceau).

Received June 15, 2017; revised September 5, 2017; accepted September 15, 2017; published OnlineFirst September 18, 2017.

REFERENCES

1. Hugo W, Shi H, Sun L, Piva M, Song C, Kong X, et al. Non-genomic and immune evolution of melanoma acquiring MAPKi resistance. Cell 2015;162:1271–85.
2. Moriceau G, Hugo W, Hong A, Shi H, Kong X, Yu CC, et al. Tunable-combinatorial mechanisms of acquired resistance limit the efficacy of BRAF/MEK cotargeting but result in melanoma drug addiction. Cancer Cell 2015;27:240–56.
3. Nazarian R, Shi H, Wang Q, Kong X, Koya RC, Lee H, et al. Melanomas acquire resistance to B-RAF(V600E) inhibition by RTK or N-RAS upregulation. Nature 2010;468:973–7.
4. Shi H, Hugo W, Kong X, Hong A, Koya RC, Moriceau G, et al. Acquired resistance and clonal evolution in melanoma during BRAF inhibitor therapy. Cancer Discov 2014;4:80–93.
5. Shi H, Moriceau G, Kong X, Koya RC, Nazarian R, Pupo GM, et al. Pre-existing MEK1 exon 3 mutations in V600E/KBRAF melanomas do not confer resistance to BRAF inhibitors. Cancer Discov 2012;2:414–24.
6. Shi H, Moriceau G, Kong X, Lee MK, Lee H, Koya RC, et al. Melanoma whole-exome sequencing identifies (V600E) B-RAF amplification-mediated acquired B-RAF inhibitor resistance. Nat Commun 2012;3:724.
7. Van Allen EM, Wagle N, Sucker A, Treacy DJ, Johannessen CM, Goetz EM, et al. The genetic landscape of clinical resistance to RAF inhibition in metastatic melanoma. Cancer Discov 2014;4:94–109.
8. Wagle N, Emery C, Berger MF, Davis MJ, Sawyer A, Pochanard P, et al. Dissecting therapeutic resistance to RAF inhibition in melanoma by tumor genomic profiling. J Clin Oncol 2011;29:3085–96.
9. Wagle N, Van Allen EM, Treacy DJ, Frederick DT, Cooper ZA, Taylor-Weiner A, et al. MAP kinase pathway alterations in BRAF-mutant melanoma patients with acquired resistance to combined RAF/MEK inhibition. Cancer Discov 2014;4:61–8.
10. Das Thakur M, Salangsang F, Landman AS, Sellers WR, Pryer NK, Levesque MP, et al. Modelling vemurafenib resistance in melanoma reveals a strategy to forestall drug resistance. Nature 2013;494:251–5.
11. Amann VC, Hoffmann D, Mangana J, Dummer R, Goldinger SM. Successful retreatment with combined BRAF/MEK inhibition in metastatic BRAFV600-mutated melanoma. J Eur Acad Dermatol Venereol 2017;82:25–26.
12. Rogiers A, Wolter P, Bechter O. Dabrafenib plus trametinib rechallenge in four melanoma patients who previously progressed on this combination. Melanoma Res 2017;27:164–7.
13. Romano E, Pradervand S, Paillusson A, Weber J, Harshman K, Muehlethaler K, et al. Identification of multiple mechanisms of resistance to vemurafenib in a patient with BRAFV600E-mutated cutaneous melanoma successfully rechallenged after progression. Clin Cancer Res 2013;19:5749–57.
14. Roux J, Pages C, Malouf D, Basset Seguin N, Madjlessi N, Baccard M, et al. BRAF inhibitor rechallenge in patients with advanced BRAF V600-mutant melanoma. Melanoma Res 2015;25:559–63.
15. Seghers AC, Wilgenhof S, Lebbe C, Neyns B. Successful rechallenge in two patients with BRAF-V600-mutant melanoma who experienced previous progression during treatment with a selective BRAF inhibitor. Melanoma Res 2012;22:466–72.
16. Seifert H, Fisher R, Martin-Liberal J, Edmonds K, Hughes P, Khabra K, et al. Prognostic markers and tumour growth kinetics in melanoma patients progressing on vemurafenib. Melanoma Res 2016;26:138–44.
17. Schreuer M, Jansen Y, Planken S, Chevolet I, Seremet T, Kruse V, et al. Combination of dabrafenib plus trametinib for BRAF and MEK inhibitor pretreated patients with advanced BRAFV600-mutant melanoma: an open-label, single arm, dual-centre, phase 2 clinical trial. Lancet Oncol 2017;18:464–72.
18. Yao Z, Torres NM, Tao A, Gao Y, Luo L, Li Q, et al. BRAF mutants evade ERK-dependent feedback by different mechanisms that determine their sensitivity to pharmacologic inhibition. Cancer Cell 2015;28:370–83.
19. Hatzivassiliou G, Song K, Yen I, Brandhuber BJ, Anderson DJ, Alvarado R, et al. RAF inhibitors prime wild-type RAF to activate the MAPK pathway and enhance growth. Nature 2010;464:431–5.
20. Heidorn SJ, Milagre C, Whittaker S, Nourry A, Niculescu-Duvas I, Dhomen N, et al. Kinase-dead BRAF and oncogenic RAS cooperate to drive tumor progression through CRAF. Cell 2010;140:209–21.
21. Poulikakos PI, Zhang C, Bollag G, Shokat KM, Rosen N. RAF inhibitors transactivate RAF dimers and ERK signalling in cells with wild-type BRAF. Nature 2010;464:427–30.
22. Su F, Viros A, Milagre C, Trunzer K, Bollag G, Spleiss O, et al. RAS mutations in cutaneous squamous-cell carcinomas in patients treated with BRAF inhibitors. N Engl J Med 2012;366:207–15.
23. Flaherty KT, Robert C, Hersey P, Nathan P, Garbe C, Milhem M, et al. Improved survival with MEK inhibition in BRAF-mutated melanoma. N Engl J Med 2012;367:107–14.
24. Dummer R, Schadendorf D, Ascierto P, Arance A, Dutriaux C, Maio M, et al. Results of NEMO: A phase III trial of binimetinib (BINI) vs. dacarbazine (DTIC) in NRAS-mutant cutaneous melanoma. J Clin Oncol 2016;34:abstr 9500.
25. Villanueva J, Infante JR, Krepler C, Reyes-Uribe P, Samanta M, Chen HY, et al. Concurrent MEK2 mutation and BRAF amplification confer resistance to BRAF and MEK inhibitors in melanoma. Cell Rep 2013;4:1090–9.
26. Conrad M, Angeli JP, Vandenabeele P, Stockwell BR. Regulated necrosis: disease relevance and therapeutic opportunities. Nat Rev Drug Discov 2016;15:348–66.
27. Dummer R, Schadendorf D, Ascierto PA, Arance A, Dutriaux C, Di Giacomo AM, et al. Binimetinib versus dacarbazine in patients with advanced NRAS-mutant melanoma (NEMO): a multicentre, open-label, randomised, phase 3 trial. Lancet Oncol 2017;18:435–45.
28. Burd CE, Liu W, Huynh MV, Waqas MA, Gillahan JE, Clark KS, et al. Mutation-specific RAS oncogenicity explains NRAS codon 61 selection in melanoma. Cancer Discov 2014;4:1418–29.
29. Davies H, Glodzik D, Morganella S, Yates LR, Staaf J, Zou X, et al. HRDetect is a predictor of BRCA1 and BRCA2 deficiency based on mutational signatures. Nat Med 2017;23:517–25.
30. Song C, Piva M, Sun L, Hong A, Moriceau G, Kong X, et al. Recurrent tumor cell–intrinsic and –extrinsic alterations during MAPKi-induced melanoma regression and early adaptation. Cancer Discov 2017;7:1248–65.
31. Kim D, Pertea G, Trapnell C, Pimentel H, Kelley R, Salzberg SL. TopHat2: accurate alignment of transcriptomes in the presence of insertions, deletions and gene fusions. Genome Biol 2013;14:R36.
32. Mathelier A, Fornes O, Arenillas DJ, Chen CY, Denay G, Lee J, et al. JASPAR 2016: a major expansion and update of the open-access database of transcription factor binding profiles. Nucleic Acids Res 2016;44:D110–5.
33. Hanzelmann S, Castelo R, Guinney J. GSVA: gene set variation analysis for microarray and RNA-seq data. BMC Bioinformatics 2013;14:7.

Published OnlineFirst September 18, 2017; DOI: 10.1158/2159-8290.CD-17-0682

AACR American Association for Cancer Research

CANCER DISCOVERY

Exploiting Drug Addiction Mechanisms to Select against MAPKi-Resistant Melanoma

Aayoung Hong, Gatien Moriceau, Lu Sun, et al.

Cancer Discov 2018;8:74-93. Published OnlineFirst September 18, 2017.